Adoptive cell therapy using T cell receptors equipped with ICOS yields durable anti-tumor response

Alexandre Marraffa[1], Cor Berrevoets[1], Margherita Mosiello[1], Rebecca Wijers[1], Daphne Roelofs[2], Mandy van Brakel[1], Kim Kroese[2], Marlies J.W. Peeters[1], Willem A. Dik[3], Andre Kunert[1], Rachel J.M. Abbott[2], Dora Hammerl[2], Christopher Schliehe[4], Reno Debets[1#]

[1]Laboratory of Tumor Immunology, Department of Medical Oncology, Erasmus MC, Rotterdam, the Netherlands, [2]Pan Cancer T BV, Rotterdam, the Netherlands, [3]Laboratory of Medical Immunology, Department of Immunology, Erasmus MC, Rotterdam, the Netherlands; [4]Department of Immunology, Erasmus MC, Rotterdam, the Netherlands.

corresponding author: (j.debets@erasmusmc.nl)

Highlights

Newly designed co-stimulatory TCR, with extracellular TCR-V and C domains coupled to CD28 transmembrane domain, and ICOS and CD3ε intracellular domains (in short TCR:ICOS) provides:

- durable anti-tumor response and T cell persistence in mouse model
- inflammatory T cell phenotype and resistance to T cell exhaustion
- effects via PI3K and NFκB activation
- translation to human T cells upon single amino acid mutation in TCR:ICOS tail
- extension to multiple clinically relevant TCRs while preserving prolonged T cell fitness

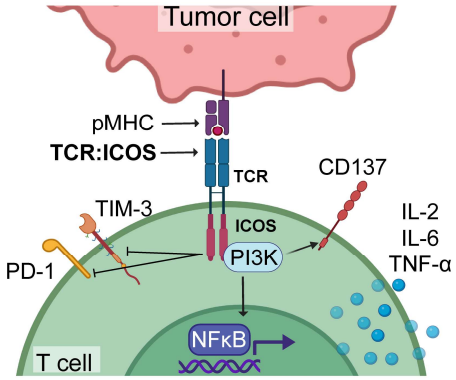

Abstract

Treatment with adoptively transferred T cells is challenged by limited longevity of therapeutic cells within tumors. To enhance the durability of anti-tumor T cell products, we have created T cell receptors (TCRs) with built-in co-stimulatory molecules. We observed that TCRs coupled to ICOS mediated exceptionally long-term responses including delay of tumor recurrence and cures in a mouse tumor model. TCR:ICOS T cells showed enhanced and antigen-specific production of inflammatory cytokines and resistance to exhaustion. Genetic ablation of ICOS-mediated activation of the PI3K-NFκB pathway neutralized the long-term anti-tumor effects. To translate TCR:ICOS to human T cells, we identified a single amino acid change in the cytosolic tail which was necessary for functional surface expression. Notably, the optimized receptor sustained performance of human T cells upon repeated stimulation across multiple antigen specificities. Collectively, we present a novel and uniformly applicable TCR:ICOS format that supports fitter T cell products for adoptive cell therapy.

Keywords: co-stimulatory TCR-T cell, immunotherapy, tumor immunology, gene engineering, solid tumors

42 **Introduction**

43 Adoptive cell therapy to treat cancer relies on the infusion of tumor-specific T cells that
44 subsequently trace and kill tumor cells. Besides non-modified T cells, such as tumor-infiltrating
45 lymphocytes (TILs) that are directed against cancer antigens via endogenous T cell receptors
46 (TCRs), T cells are often derived from blood and redirected toward cancer antigens via gene-
47 engineering with chimeric antigen receptors (CARs) or TCRs. CAR-T cell therapy has already
48 exhibited remarkable success and achieved objective response rates up to 90% in
49 hematological malignancies (1–6). Currently, seven CAR-T cell products directed to either
50 CD19 or BCMA have received FDA approval and now constitute standard-of-care treatment
51 for B cell lymphomas and multiple myeloma (7). In addition, TIL and TCR-T cell treatments
52 have shown objective responses of over 40% in solid tumors, such as melanoma and synovial
53 sarcoma (8,9). This has led to the 2024 FDA approval of a TIL product directed against
54 melanoma and a TCR-T cell product directed against synovial sarcoma antigen MAGE-A4
55 (10). Despite this tremendous progress, there is still an urgent need to identify gene-
56 engineering strategies to enhance T cell fitness, particularly for the treatment of solid tumors,
57 where the long-term efficacy of T cell therapy is lagging behind that of hematological
58 malignancies.

59 A major cause of ineffective or transient clinical effects is the inability of adoptively transferred
60 T cells to sufficiently resist the immunosuppressive tumor microenvironment (TME). Multiple
61 reports have already demonstrated that within TMEs, T cells become progressively
62 dysfunctional, show a curtailed persistence as well as a diminished anti-tumor activity, as
63 reviewed in (11–13). In addition, the inhospitable TME impairs T cell infiltration, migration and
64 antigen presentation to T cells, which, together, significantly limit the durability of anti-tumor T
65 cells (12). Specifically, TMEs lack sufficient co-stimulatory ligands, thereby preventing optimal
66 T cell activation and potentially initiating T cell impairments (14,15). In fact, negligible
67 expression of co-stimulatory ligands, often accompanied by an overabundance of co-inhibitory
68 ligands, may mirror TMEs that are the result of adaptive feedback mechanisms that hamper

69 the longevity of anti-tumor T cells (16–19). To bypass the need for exogenous, i.e. TME-
70 derived co-stimulation, we propose to create TCRs with built-in co-stimulatory molecules,
71 thereby providing a second signal upon antigen recognition. Although clinical CARs already
72 contain co-stimulatory domains, engineering co-stimulatory TCRs with the potential to unlock
73 T cell therapy for a large collection of targets, is an underexplored strategy. In fact, engineering
74 TCRs, in contrast to CARs, faces typical structural constraints due to the necessary assembly
75 of TCR chains with CD3 components as well as the requirement to bind peptide:MHC
76 complexes.

77 In the present study, we have developed a panel of new TCRs incorporating co-stimulatory
78 molecules and evaluated these TCR-T cells for durability of the anti-tumor effect in an
79 aggressive melanoma mouse model. The TCR harboring Inducible T cell Co-Stimulator
80 (TCR:ICOS) resulted in exceptionally long-term cures and delay of tumor recurrence and was
81 identified as the lead candidate. Subsequently, we uncovered its mechanism of action by
82 performing a series of *in vivo* and *in vitro* experiments. Finally, we translated the murine
83 TCR:ICOS format for its use in human T cells and demonstrated its surplus value regarding T
84 cell longevity across multiple clinically relevant antigen specificities.

85

86 **Materials and Methods**

87 *Design of murine co-stimulatory TCRs*

88 TCRα and β genes specific for the human gp100$_{280-288}$ epitope (YLEPGPVTA) presented by
89 HLA-A2 (gp100/A2) were derived from clone CTL-296 (20), murinized and codon-optimized
90 as described earlier (21). Subsequently, TCR genes were cloned into the pMP71 vector (a
91 kind gift of Prof. Wolfgang Uckert, MDC, Berlin, Germany (22)), in which the TCRα and β
92 chains were separated by an optimized T2A ribosome skipping sequence according to a
93 TCRß-T2A-TCRα format, as described before (23). Murine TCR:CD28 was generated as
94 described in Govers et al., 2014 (24). Shortly, human (h)TCR-Vα was coupled to mouse
95 (m)TCR-Cα and hTCR-Vß to mTCR-Cß (all extracellular domains), and each TCR chain was
96 followed by a proline-lysine (PK) linker, the mCD28 transmembrane, mCD28 intracellular and
97 mCD3ε intracellular domains. Murine OX40, ICOS and 4-1BB intracellular domains were
98 ordered via GeneArt (Life Technologies) and introduced into the TCR:CD28 cassette
99 (replacing the intracellular domain of CD28) via overlap PCR with use of Q5 High Fidelity DNA
100 Polymerase (New England Biolabs). One variant to TCR:ICOS with an amino acid substitution
101 in ICOS (Y181F), named TCR:ICOS-YF, was designed by site directed mutagenesis of Y181F
102 in the mICOS domain to prevent docking and downstream signaling of PI3K, as described
103 before by Gigoux et al. (25). Sequences were obtained and checked using the BigDye
104 Terminator v3.1 Cycle Sequencing Kit (Applied Biosystems) and the ABI sequence analyzer.
105 All mTCRs used in this study are schematically depicted in **Figures 1a** and **4a**. Primer
106 sequences can be obtained upon request.

107

108 *Design of human co-stimulatory TCRs*

109 To convert the gp100/A2 mTCR:ICOS into a human format (hTCR:ICOS), we generated the
110 pMP71 vector consisting of gp100/A2 hTCR-VDJß-Cß-T2A-hTCR-VJα-Cα (extracellular
111 domains), and in which each TCR chain was followed by a proline-lysine (PK) linker, the

112 hCD28 transmembrane, the hICOS intracellular and hCD3ε intracellular domains. This
113 hTCR:ICOS construct demonstrated poor surface expression in human T cells (see
114 **Supplementary Figure 6a**). To identify which building blocks (or combinations thereof) and/or
115 which amino acid boundaries of such building blocks determine functional expression of
116 TCR:ICOS in human T cells, a panel of 49 variants was designed (all produced by GeneArt),
117 and tested for surface expression in a stepwise approach. An overview of the different
118 constructs, including detailed specifics, is provided in **Supplementary Table 1**. In all
119 transduction experiments, the wt TCR was taken along as a reference. A scheme of the study
120 design to select and test hTCR:ICOS variants is shown in **Figure 6a**. Following selection of
121 hTCR:ICOS-RA, in which the mutation R54A was introduced in the hCD3ε domain (**Figure**
122 **6c)**, this construct was further tested for antigen recognition, sensitivity, cytotoxicity and
123 performance upon repeated antigen stimulation. To test the applicability of hTCR:ICOS-RA to
124 other TCR specificities, the gp100/A2 TCR-Vα and Vß domains were exchanged with those
125 of the TCR directed against NY-ESO1/A2 and against Ropporin-1/A2 (ROPN1, all new
126 constructs were produced by GeneArt) (26–28). The NY-ESO1 hTCR:ICOS-RA and the
127 ROPN1 hTCR:ICOS-RA were tested again for surface expression, antigen recognition,
128 sensitivity and performance upon repeated antigen stimulation.

129 *Retroviral transduction of TCRs into T cells*

130 Mouse T cell transductions were performed as previously described by Pouw and colleagues
131 (21). Shortly, 293T and Ph-A packaging cells were transfected with pHit60 MLV GAG/POL
132 and pHit123 ENV helper constructs (29), and the TCR of interest, using calcium phosphate
133 (Promega Profection Mammalian Transfection system). Mouse splenocytes were isolated,
134 activated for 24h with 0.5µg/mL Concavalin A (Sigma) and exposed once to virus supernatant
135 produced by the packaging cells. Human T cell transductions were performed as previously
136 described by Lamers and colleagues (30). In this case, 293T and Ph-A packaging cells were
137 transfected with pHit60 MLV GAG/POL and pColtGalV ENV helper constructs (31), and the
138 TCR of interest, using the procedure described above. Human PBMCs were activated for 48h

139 using 10 ng/mL soluble anti-CD3 antibody (OKT3, Thermo Fisher Scientific) before being
140 exposed twice to virus supernatant. TCR expression levels were determined using flow
141 cytometric detection of the introduced TCR-Vß, corrected for percentage positivity as
142 observed with mock-transduced T cells from the same donor, and displayed as % positive
143 cells within the CD3+ T cell population. In experiments measuring killing ability of human TCR
144 T cells, a protocol adapted from a Good Manufacturing Practice (GMP) protocol was followed,
145 as described before (32). Shortly, human PBMCs, isolated from buffy coats obtained from
146 Sanquin (Amsterdam, the Netherlands), were activated with 30 ng/mL soluble anti-CD3
147 (OKT3, Miltenyi Biotec) and 30 ng/mL anti-CD28 (clone 15E8, Miltenyi Biotec), 110 IU/mL
148 hIL15 (Miltenyi Biotec), and 0.1 IU/mL hIL21 (Miltenyi Biotec) in X-vivo 15 medium (Lonza)
149 containing 2% Human Serum for 48h before being exposed twice to virus supernatant.

150 *Adoptive cell therapy*

151 C57BL/6 HHD mice expressing the chimeric A2:K^b molecule (33) were bred at Erasmus MC
152 and were used for adoptive T cell experiments as described previously with minor adaptations
153 (24). Shortly, mice were transplanted with $0.5x10^6$ cells of the B16:HHD-YLE clone 18 to 25
154 days prior to T cell transfer at day 0. TCR T cells (6 to $7.5x10^6$ cells) were transferred
155 intravenously, preceded by myeloablation through intraperitoneal injections of busulphan
156 (16.5 µg/kg on days -4 and -3; Sigma) and cyclophosphamide (200 mg/kg on day -2; Sigma).
157 For mock T cells, the same total number of cells was transferred as for wt TCR T cells. Tumor
158 volumes were measured three times per week using a caliper and calculated using the formula
159 0.4 x (AxB^2), where A represents the largest diameter measured, and B^2 the perpendicular
160 diameter (34). Tumor regression was defined as decreases in tumor volume of at least 30%
161 after T cell transfer, whereas tumor relapse was defined as increases in tumor volume at 3
162 consecutive measurements after the initial tumor regression. Anti-tumor responses of mice at
163 115 days post-treatment were categorized as follows: a complete response as 100 % initial
164 tumor regression with tumor remaining non-palpable; partial response as tumor regression
165 followed by a tumor relapse; and non-response no tumor regression. 3-4 mice with regressing

166 tumors 5 days after T cell transfer were sacrificed, and tumors were used for RNA sequencing
167 (following snap freezing and storage at -80ºC) as well as flow cytometric phenotyping of TILs
168 (after making single cell suspensions). Mice were sacrificed when the tumor burden exceeded
169 1400 mm^3, at which point relapsed tumors were collected. Blood samples were collected from
170 the tail vein at weekly intervals for 11-16 weeks after T cell transfer and used for flow
171 cytometric counting and phenotyping of TCR T cells.

172 *Detection of intracellular phosphorylation*

173 Mouse T cells expressing either wt TCR or TCR:ICOS ($6x10^4$ cells/well) were co-cultured with
174 the B16:HHD-YLE clone or B16F10 wt ($2x10^4$ cells/well) in Complete Mouse Medium in a
175 tissue culture-treated 96-well plate at 37°C. After 2h, cells were fixed and stained and
176 assessed for pPI3K (as described under 'flow cytometry'). To assess the ability of TCR:ICOS
177 to phosphorylate a large array of intracellular substrates, we treated wells from a non-tissue
178 culture 96-well plate that were streptavidin pre-coated (Pierce) with 50µL of 1mg/mL
179 biotinylated A2:Kb pentamer fused to the gp100 peptide YLEPGPVTA or an irrelevant peptide
180 (FLYTYIAKV, Proimmune) for 1h at RT, after which wells were washed three times with PBS
181 + 0.5% Tween-20 (Sigma). Mouse T cells expressing either gp100/A2 wt TCR, TCR:ICOS or
182 TCR:ICOS-YF were added to the plates ($0.25x10^6$ cells/well in 50µL Cytotox medium) for 30
183 min at 37°C, with frequencies of TCR-expressing T cells after transduction normalized towards
184 TCR:ICOS T cells using Mock T cells. Following pMHC stimulations, plates were placed on
185 ice and T cells were harvested and lysed with lysis beads, after which proteins were extracted,
186 biotinylated and placed on the antibody array, followed by the addition of a Cy3-Streptavidin
187 dye (GEPA43001, Merck) according to the manufacturer's instructions (antibody array assay
188 kit KAS02 and T cell Receptor Phospho-Antibody Array PTC188, Fullmoon Biosystems). To
189 validate the effect of stimulation, one well from each condition was kept separate for flow
190 cytometric detection of pERK1/2 (see above, and **Supplementary Figure 4b**). Detection of
191 the Cy3 signal was performed using a Typhoon 5 fluorescent scanner and quantified using
192 Imagequant TL with normalization according to the running ball background subtraction tool

193 (Fiji, ImageJ 1.53t). Downstream analysis was performed using R, where median background
194 of each slide was subtracted from the corresponding experimental values, and replicates (n=5)
195 were averaged. Finally, the phosphorylation ratio after stimulation was calculated using the
196 following formula:

197 $$\frac{(\text{phosphorylated protein 1})/(\text{unphosphorylated protein 1})}{(\text{phosphorylated protein 2})/(\text{unphosphorylated protein 2})}$$

198 where 1 refers to the stimulated condition and 2 to the unstimulated condition. The different
199 phosphorylated proteins were then classified into main T cell signaling pathways based on
200 literature.

201 *Release of inflammatory cytokines*

202 Mouse T cells expressing either wt TCR, TCR:ICOS or TCR:ICOS-YF ($0.75x10^6$ cells/well)
203 were co-cultured with the melanoma cell clone B16:HHD-YLE or B16F10 wt cells ($0.25x10^6$
204 cells/well) in Complete Mouse Medium in a tissue culture treated 24-well plate for 16h at 37°C.
205 Mock T cells served as negative controls. Supernatants were assessed for the presence of
206 cytokines (according to a customized Luminex assay, R&D Systems Minneapolis USA;
207 measuring IFN-γ, IL-1ß, IL-2, IL-4, IL-5, IL-6, IL-10, IL-17, CCL5, CCL20, CXCL2, MMP-8,
208 MMP-9 and TNF-α). Values outside of range and not extrapolatable were excluded.

209 *Repeated stimulations with tumor cells*

210 Mouse TCR T cells expressing either wt TCR, TCR:ICOS or TCR:ICOS-YF ($0.75x10^6$) were
211 co-cultured with B16:HHD-YLE or B16F10 wt cells ($0.25x10^6$ cells) in Complete Mouse
212 Medium supplemented with 25 IU/mL IL-2 in a 24-well plate for 16h at 37°C, with frequencies
213 of TCR-expressing T cells after transduction normalized towards TCR:ICOS T cells using
214 Mock T cells. After this 1st cycle of exposure, T cells were harvested with 20% of the sample
215 being exposed to flow cytometric detection of T cell PD1 and TIM3, and 80% of the sample
216 being again co-cultured for the 2nd cycle. Tumor cells were freshly pre-seeded to ensure an
217 80% confluency at start of co-culture with T cells. Experiments were performed over 4 cycles

218 of 16h each. Repeated stimulation with human TCR T cells were performed in a similar
219 manner, using either BLMgp100 (using gp100/A2 TCR T cells), MM-231-ROPN1 (ROPN1/A2
220 TCR) or MM-231-NY-ESO-1 (NY-ESO-1/A2 TCR) as target cells, freshly thawed T cells as
221 effector cells, and co-culturing the cells in T cell medium supplemented with 50 IU/mL IL-2.

222 *Detection of antigen reactivity and sensitivity of TCR T cells*

223 To assess antigen reactivity of murine TCR T cells, T cells expressing either wt TCR, or a co-
224 stimulatory TCR ($6x10^4$ cells/well) were co-cultured with B16-HHD-YLE in Cytotox medium in
225 a tissue culture treated 96-well plate for 16h at 37°C. B16wt cells as well as Mock T cells were
226 used as negative controls. To assess antigen sensitivity, TCR T cells ($6x10^4$ cells/well) were
227 co-cultured with B16-HHD cells ($2x10^4$ cells/well) pretreated with 10µg/mL mIFN-γ (Sanquin)
228 24h prior to stimulation and loaded with cognate peptide (gp100 peptide) at increasing
229 concentrations (from 0.1 nM to 30 µM) in Cytotox medium in a tissue culture treated 96-well
230 plate for 16h at 37°C. Supernatants were assessed for the presence of mIFN-γ by enzyme-
231 linked immunosorbent assay (ELISA, Biolegend). To assess antigen reactivity of human TCR
232 T cells, T cells expressing either wt TCR or TCR:ICOS-RA ($6x10^4$ cells/well) were co-cultured
233 with BLM-gp100 (gp100/A2 TCR), MM-231-ROPN1 (ROPN1/A2 TCR) or MM-231-NY-ESO1
234 (NY-ESO1/A2 TCR) in Cytotox medium in a tissue culture treated 96-well plate for 16h at
235 37°C. BLM wt and MM-231 wt cell lines as well as Mock T cells were used as negative controls.
236 To assess antigen sensitivity, TCR T cells ($6x10^4$ cells/well) were co-cultured with T2 cells
237 ($2x10^4$ cells/well) loaded with cognate peptide (gp100, NY-ESO-1 or ROPN1 peptide) at
238 increasing concentrations (from 0.1 nM to 30 µM) in Cytotox medium in a tissue culture treated
239 96-well plate for 16h at 37°C. Supernatants were assessed for the presence of hIFN-γ by
240 enzyme-linked immunosorbent assay (ELISA, Biolegend).

241 *Detection of tumor cell killing ability of human TCR T cells*

242 To assess killing ability of human TCR:ICOS T cells, BLM-gp100-eGFP ($16x10^3$ cells), MM-
243 231-ROPN1-eGFP ($32x10^3$ cells) or MM-231-NY-ESO1-eGFP ($16x10^3$ cells) were seeded

244 onto wells from a flat bottom tissue culture treated 96 well plate (Falcon) in T cell medium
245 supplemented with 50 IU/mL IL-2 overnight to reach a confluency of 50-80%. Human T cells
246 expressing either wt TCR or hTCR:ICOS directed to either hgp100, NY-ESO1 or ROPN1 were
247 thawed and co-cultured with their respective targets in an Incucyte SX5 placed inside a 37°C,
248 5% CO_2 incubator ($144x10^3$ cells/well targeting gp100, $96x10^3$ cells/well targeting ROPN1 and
249 $32x10^3$ cells/well targeting NY-ESO1). Pictures of the wells were taken every 4h and GFP-
250 covered areas were determined. Each experimental condition was run in quintuplicate and
251 mock transduced T cells were used as negative controls.

252 *Statistical analyses*

253 Statistical analysis and data display was performed using either GraphPad Prism (GraphPad
254 Software, La Jolla, CA, version 8.0.2) or Rstudio (version 4.3.1). Statistical tests were
255 considered significant when $p<0.05$. Changes in tumor volume or number of T cells over time
256 were compared according to linear mixed models, with correction for random effect and
257 elapsed time as a separate variable. All treatments were compared to the wt TCR condition
258 and the interaction between treatment effect and time elapsed was reported. Survival of
259 responding mice was compared according to the Cox regression model. Multiple group
260 comparisons were performed either with 2-way ANOVA or, when the requirements were not
261 met, Kruskal-Wallis test. Post-hoc testing was performed either with t-tests (if needed with
262 Dunnets or Holm Sidak's correction) or Dunns' test.

263 For further description of materials and methods, particularly regarding cell culture, flow
264 cytometry and RNA transcriptomics, see supplementary text.
265

266 **Results**

267 *TCR:ICOS mediates durable anti-melanoma T cell responses*

268 We designed a panel of co-stimulatory TCRs, all directed against the HLA-A2-restricted
269 melanoma epitope $gp100_{280-288}$. These new TCRα and β chains each consisted of the
270 extracellular human variable and murine constant domains of the TCR, followed by the murine
271 CD28 transmembrane domain, the intracellular domains of either murine CD28, CD134
272 (OX40), CD137 (4-1BB) or CD278 (ICOS) and the murine CD3ε intracellular domain (**Figure**
273 **1a**). This new design extended our previous observation that the transmembrane domain of
274 CD28 and, downstream, the intracellular tail of CD3ε are beneficial for functional surface
275 expression (24). All co-stimulatory TCRs were successfully transduced in murine T cells,
276 except for the TCR with the 4-1BB domain, which showed very low surface expression, and
277 was therefore excluded from further experiments (**Supplementary Figure 1a**). Co-stimulatory
278 TCRs were next tested for antigen reactivity and sensitivity *in vitro*, which demonstrated
279 antigen-specific IFN-γ production, although for all co-stimulatory TCR T cells with a lower
280 avidity than wild-type (wt) TCR T cells (**Supplementary Figure 1b and c**). Subsequently,
281 these TCRs were assessed in a mouse model for adoptive cell therapy, where B16:HHD-YLE
282 melanoma cells overexpressing the cognate antigen were transplanted into immune
283 competent HHD mice and T cells were transferred once the tumor became palpable (**Figure**
284 **1b**). Notably, while treatment with all TCR T cell products provided an initial tumor regression,
285 only treatment with TCR:ICOS T cells provided an unambiguous advantage over wt TCR T
286 cells (**Figure 1c**). In fact, treatment with TCR:ICOS T cells led to significantly increased
287 survival, with 60% of the mice surviving as long as 150 days after T cell transfer compared to
288 0% for wt TCR and TCR:CD28 and 16% for TCR:OX40 T cells (**Figure 1d**). Moreover, mice
289 treated with TCR:ICOS T cells showed a longer median time to relapse than those treated
290 with other TCR T cells (140 days for TCR:ICOS vs 22, 32 and 35 days for wt TCR, TCR:OX40
291 and TCR:CD28, respectively, **Figure 1e**). Remarkably, when assessing the extent of response
292 (i.e., complete, partial or non), TCR:ICOS T cell-treated mice had the highest rate of complete

293 responders (i.e., 43% for TCR:ICOS vs 14, 0 and 0% for TCR:OX40, TCR:CD28 and wt TCR,
294 **Supplementary Figure 1e)**. The durable anti-tumor response observed for mice treated with
295 TCR:ICOS T cells was accompanied by a long-term persistence of circulating CD8 T cells
296 expressing the introduced TCR (median of 119, 77 and 4 TCR+ CD8 T cells per μL blood at
297 100 days post-treatment for TCR:ICOS, TCR:OX40 and wt TCR, measurement not applicable
298 for TCR:CD28 due to absence of surviving mouse **Figure 1f**). Of note, the relative long-term
299 persistence observed with TCR:OX40 T cells was due to a single mouse showing persistent
300 T cells. The enhanced persistence of TCR:ICOS T cells was also observed for CD4 T cells,
301 albeit to a lesser extent (**Supplementary Figure 1d**). Taken together, these results
302 demonstrate a superior *in vivo* durability of anti-melanoma responses, accompanied by a
303 prolonged persistence of transferred T cells mediated by TCR:ICOS compared to alternative
304 co-stimulatory TCRs.

305

306 *Intra-tumoral TCR:ICOS CD8 T cells exhibit a young and co-stimulatory phenotype*

307 Next, we focused on TCR:ICOS and investigated whether its impact on the durability of anti-
308 tumor responses was associated with the phenotype of circulating and tumor-infiltrating T
309 cells, specifically their maturation state and expression of co-signaling receptors
310 (schematically displayed in **Figure 2a**). When analyzing peripheral blood at 21 days post-
311 treatment, we observed that TCR+ CD8 T cells from both TCR:ICOS and wt TCR T cell-treated
312 mice were highly differentiated with the majority of cells expressing “antigen-experience”
313 markers such as 4-1BB and displaying an effector memory phenotype with no clear
314 differences between the two groups (**Figure 2b**). In addition, we observed low fractions of
315 circulating TCR+ CD8 T cells co-expressing two or more co-inhibitory receptors and large
316 fractions co-expressing two or more co-stimulatory receptors, again with no clear differences
317 between the two treatment conditions. For instance, 16% of TCR:ICOS+ CD8 T cells and 17%
318 of wt TCR+ CD8 T cells co-expressed PD1 and TIM3, whereas 76% of TCR:ICOS+ and 78%
319 of wt TCR+ CD8 T cells co-expressed CD40L and 4-1BB. Also, circulating CD4 T cells showed

320 similar patterns with little to no difference observed between treatment groups
321 (**Supplementary Figure 2a**). In contrast, when analyzing regressing tumors at five days post-
322 treatment, we observed that TCR:ICOS+ CD8 TILs exhibited a higher proportion of cells with
323 a young naïve-like or central memory state and significantly fewer with a more differentiated
324 effector memory state when compared to wt TCR+ CD8 TILs (**Figure 2c,** right panel). Notably,
325 a larger proportion of TCR:ICOS+ CD8 TILs expressed 4-1BB and OX40, either as a single
326 receptor, together or in combination with another co-stimulatory receptor relative to wt TCR+
327 CD8 TILs (**Figure 2c**, middle panel). With respect to CD4 TILs, treatment with TCR:ICOS T
328 cells was characterized by a significantly higher fraction of cells expressing TIM3 and CTLA4
329 when compared to treatment with wt TCR+ T cells (**Supplementary Figure 2b)**. Moreover,
330 we noted a higher frequency of co-stimulatory receptor-expressing TCR:ICOS+ CD4 TILs
331 versus wt TCR+ CD4 TILs, even though differences did not reach statistical significance due
332 to low numbers of TCR+ CD4 TILs measured. Collectively, these results show that while
333 TCR:ICOS T cells are more abundant in the blood of mice, phenotypic differences of these
334 cells were restricted to tumors, where TCR:ICOS+ CD8 TILs, but not wt TCR+ CD8 TILs,
335 feature a young and co-stimulatory phenotype.

336

337 *TCR:ICOS T cells create an inflammatory micro-environment in tumors*

338 Subsequently, we performed transcriptional profiling of tumors following treatment with either
339 TCR:ICOS T cells or wt TCR T cells. Interestingly, genes that were differentially expressed in
340 tumors that regressed after treatment with TCR:ICOS versus wt TCR T cells were to a large
341 extent immune-related (e.g., Cxcl2, Il1b or Ccl5), indicative of a more inflammatory TME in
342 TCR:ICOS-treated mice (**Figure 3a)**. In line with this, gene set enrichment analysis highlighted
343 that “inflammatory response” was the most enriched pathway in regressing tumors from
344 TCR:ICOS but not wt TCR T cell-treated mice (**Figure 3b)**. Additionally, the pathways “IL6
345 JAK STAT signaling” and “TNF-α signaling via NFκB” were also highly enriched in these
346 tumors, further supporting the notion that TCR:ICOS T cells promote an inflammatory TME, at

347 least in part through activation of the NFκB pathway. In contrast, transcriptomic analysis of
348 relapsed tumors following treatment with TCR:ICOS T cells showed no significant enrichment
349 of these or any other gene set compared to wt TCR T cells, indicating that treatment with
350 TCR:ICOS T cells induced changes early-on, which were lost when tumors relapsed
351 (**Supplementary Figure 3a**). In extension to this observation, the scores of various immune-
352 related signatures that associate with either T cell infiltration, antigen presentation or T cell
353 function (35,36) were reduced in relapsed versus regressed tumors (**Supplementary Figure**
354 **3b**). These findings, at the level of gene expression in tumors, suggest that TCR:ICOS T cells
355 induce a local inflammatory TME.

356

357 *In vitro stimulated TCR:ICOS T cells activate the NFκB pathway, produce inflammatory*
358 *cytokines and are resistant to exhaustion upon repeated tumor cell exposure*

359 To test the mechanism of action of TCR:ICOS T cells toward the observed pro-inflammatory
360 TME, we performed a series of *in vitro* assays. In preparation for these experiments, we
361 confirmed activation-dependent phosphorylation of PI3K, a recognized target of ICOS,
362 following stimulation with the tumor cell clone B16:HHD-YLE (the same as used for *in vivo*
363 experiments, **Supplementary Figure 4a**). TCR:ICOS CD8 T cells showed significantly higher
364 levels of phosphorylated PI3K (pPI3K) compared to wt TCR T cells. We also generated a
365 TCR:ICOS-YF mutant in which the tyrosine of the active domain of ICOS was mutated into a
366 phenylalanine, thereby abrogating activation of PI3K and its downstream substrates (**Figure**
367 **4a**) (25).

368 In a first series of experiments, T cells expressing either wt TCR, TCR:ICOS or TCR:ICOS-
369 YF were stimulated with immobilized A2Kb chimeric MHC molecules coupled to the gp100
370 peptide or an irrelevant peptide for 30 minutes after which cell lysates were exposed to a
371 kinase microarray. The occurrence of T cell activation was validated by detecting an increase
372 in the fraction of TCR T cells positive for pERK1/2 (**Supplementary Figures 4b**). Remarkably,

373 stimulation of TCR:ICOS T cells induced significant phosphorylation of multiple members of
374 the NFκB family, such as Rel, p100/52, p105/50, IKKα/β, IKKγ and IKBβ, which was not
375 observed in stimulated wt TCR or TCR:ICOS-YF T cells (**Figure 4b**). Expectedly, the PI3K
376 pathway, with substrates such as AKT-Y236, is activated as well upon antigen-specific
377 triggering of TCR:ICOS. The TCR or p38 pathways, harbor individual substrates that are also
378 differentially phosphorylated when comparing TCR:ICOS to wt TCR T cells, however, when
379 assessing pathways as a whole not to the same extent as the NFκB pathway. In a second
380 series of experiments, we have stimulated TCR T cells with either antigen-positive or antigen-
381 negative B16 tumor cells overnight and measured the secretion of 14 cytokines. We found
382 that TCR:ICOS T cells produced significantly higher levels of cytokines and chemokines, such
383 as IL-2, IL-6, CCL5, CXCL2 and TNF-α, in response to antigen-positive cells when compared
384 to wt TCR T cells (**Figure 4c, Supplementary Figure 4c**). Importantly, this cytokine profile
385 was not observed in T cells expressing the signaling-deficient TCR:ICOS-YF mutant. Many of
386 the cytokines with enhanced secretion are direct downstream targets of the NFκB pathway
387 and play active roles in tissue inflammation (37,38). Moreover, some of these mediators, such
388 as IL-6, CCL5 and CXCL2, also showed increased gene expression in regressing tumors
389 following treatment with TCR:ICOS T cells, demonstrating strong concordance between our
390 *in vitro* and *in vivo* findings (**Figure 3a and b**). In a third series of experiments, we repeatedly
391 exposed TCR T cells to fresh antigen-positive or negative melanoma cells and assessed the
392 co-expression of PD1 and TIM3 as markers of T cell exhaustion. We found that the fraction of
393 $PD1^{+}TIM3^{+}$ CD8 T cells over 3 rounds of antigen-specific stimulation was significantly lower
394 for TCR:ICOS when compared to wt TCR or TCR:ICOS-YF T cells (**Figure 4d** and
395 **Supplementary Figure 4d**). Taken together, this series of *in vitro* experiments revealed that
396 TCR:ICOS preferentially signals through the PI3K-NFκB pathway, leading to the production of
397 inflammatory cytokines and resulting in enhanced resistance to T cell exhaustion upon
398 repeated stimulation. A proposed mechanism of action of TCR:ICOS is illustrated in
399 **Supplementary Figure 4e**.

400

401 *Durability of anti-tumor response of T cells depends on ICOS-docking site for PI3K*

402 To provide evidence that the PI3K pathway activation contributed to the *in vivo* efficacy of
403 TCR:ICOS T cells, we compared the performance of TCR:ICOS-YF (the mutant unable to
404 dock PI3K) to TCR:ICOS and wt TCR T cells in the melanoma mouse model (**Figure 5a**). Mice
405 treated with TCR:ICOS T cells exhibited effective and durable antitumor response, whereas
406 mice treated with either TCR:ICOS-YF or wt TCR T cells showed a substantially reduced
407 survival (55, 30 and 20% survival at 150 days, respectively, **Figure 5b**, **5c** and
408 **Supplementary Figure 5a**). In addition, median time to relapse was shorter in TCR:ICOS-YF
409 and wt TCR T cells groups (30 and 26 days), while it was not reached within 150 days in the
410 TCR:ICOS T cell group (**Figure 5d**). Lastly, TCR:ICOS CD8 T cells showed superior
411 persistence in blood compared to TCR:ICOS-YF and wt TCR CD8 T cells (**Figure 5e**),
412 whereas CD4 T cells exhibited lower persistence across all treatment groups (**Supplementary**
413 **Figure 5b**). These results confirm that TCR:ICOS enhances the durability of anti-melanoma
414 T cell responses through PI3K-dependent signaling.

415

416 *A single amino acid substitution in the cytosolic tail of the CD3ε domain enables functional*
417 *expression of human TCR:ICOS in human T cells*

418 In a final set of experiments, we translated our findings to a clinically relevant setting by
419 designing and stringently testing a human TCR:ICOS construct (hTCR:ICOS) for its
420 performance in human T cells. The rationale for these experiments comes from the
421 observation that gene transfer of the gp100/A2 hTCR:ICOS using orthologous human instead
422 of murine sequences for each building block resulted in low surface expression in human T
423 cells (mean ± SEM: 5 ± 1% TCR-Vβ+ cells within CD3+ T cells, n=18) when compared to the
424 murine TCR:ICOS construct (mTCR:ICOS, 17 ±3%, n=24) (**Supplementary Figure 6a and**
425 **b**). To create a functionally expressed hTCR:ICOS while maintaining its overall format, we

426 designed a panel of 50 variants to systemically test the impact of individual building blocks (or
427 combinations thereof) and/or amino acid boundaries of these building blocks on surface
428 expression in human T cells (**Figure 6a and Supplementary Table 1**). Using a stepwise
429 approach, we started by exchanging each individual building block of the mTCR:ICOS (i.e.,
430 the extracellular TCR-C, the CD28 transmembrane, the ICOS intracellular and the CD3ε
431 intracellular domains) for their human orthologues (**Figure 6b, left panel**). These mTCR:ICOS
432 variants were introduced into human T cells, and surface expression was compared to the
433 original mTCR:ICOS and wt TCR (**Figure 6b, middle panel**). While the introduction of human
434 CD28 or ICOS domains did not impair expression, that of human TCR-C or CD3ε domains led
435 to a notable lower expression (6 and 12% of TCR+ T cells, respectively, when compared to
436 18% for mTCR:ICOS). These results were re-assessed by performing the reverse experiment,
437 where starting from hTCR:ICOS the latter two domains were substituted for their murine
438 orthologues (**Figure 6b, right panel**). While introduction of the mTCR-C domain in an
439 otherwise fully human hTCR:ICOS did not rescue the surface expression of hTCR:ICOS,
440 introduction of the mCD3ε domain instead restored expression to a level comparable to that
441 of mTCR:ICOS. In the next step, we focused on the five amino acid differences between
442 human and murine CD3ε and constructed single amino acid substituents in hTCR:ICOS
443 (**Figure 6c**). Strikingly, substitution of arginine at position 54 with alanine (hTCR:ICOS-
444 CD3εR54A, in short: hTCR:ICOS-RA; corresponding to construct nº45 in **Supplementary**
445 **Table 1**), led to expression levels that exceeded those of mTCR:ICOS and were similar to
446 those of wt hTCR (35.5% for hTCR:ICOS-RA and wt hTCR vs 17.5% for mTCR:ICOS). In a
447 last step, we validated the *in vitro* efficacy of this hTCR:ICOS-RA variant, characterizing its
448 antigen sensitivity, reactivity, tumor killing ability as well as its resistance to T cell exhaustion.
449 When challenged with titrated amounts of cognate peptide, hTCR:ICOS-RA T cells showed
450 only slightly higher EC50 values and amplitude regarding IFN-γ production when compared to
451 wt TCR T cells (**Figure 6d, 2nd panel**). When stimulated with human melanoma cells that
452 express the hgp100 antigen, hTCR:ICOS-RA T cells produced IFN-γ and effectively killed
453 tumor cells (**Figure 6d**, **3rd and 4th panel**). Importantly, hTCR:ICOS-RA CD8 T cells showed

454 significantly lower fractions co-expressing PD1 and TIM3 after repeated antigen stimulation
455 compared to wt TCR T cells (**Figure 6d**, **5th panel**).

456 Having established a successful format to gene-engineer human T cells with TCR:ICOS, we
457 then evaluated whether this format could be extended to other TCR specificities targeting
458 clinically relevant antigens. To this end, we tested surface expression and *in vitro* performance
459 of hTCR:ICOS-RA directed against NY-ESO1/HLA-A2 and ROPN1/HLA-A2 (**Figure 6e** and
460 **Figure 6f**). The NY-ESO1 TCR is directed against esophageal squamous cell carcinoma 1
461 antigen and is in an advanced stage of clinical development for synovial sarcoma (26),
462 whereas the ROPN1 TCR targets Ropporin and is being developed for adoptive T cell therapy
463 to treat Triple Negative Breast Cancer (TNBC) (27). For both NY-ESO1 and ROPN1
464 hTCR:ICOS, we demonstrated an R54A substitution-dependent surface expression (**Figure**
465 **6e and f, 1st panels**). In addition, functional assays demonstrated that hTCR:ICOS-RA T cells
466 have a similar antigen sensitivity relative to wt TCR T cells and robustly recognize and kill
467 tumor cells. Lastly, and relevant to this study, hTCR:ICOS-RA CD8 T cells targeting either NY-
468 ESO1 or ROPN1 also showed lower levels of T cell exhaustion markers (PD1 and TIM3)
469 following multiple rounds of repeated antigen stimulation when compared to their wt TCR
470 counterparts. In short, we found that surface expression of hTCR:ICOS was dependent on a
471 single amino acid substitution, which preserved antigen sensitivity and recognition as well as
472 resistance to the induction of T cell exhaustion of TCRs with multiple antigen specificities.

473

474 **Discussion**

475 Our current study unveils a new TCR format that provides built-in co-stimulation through ICOS
476 and enables exceptionally prolonged anti-tumor T cell responses in an immune competent
477 melanoma mouse model. TCR:ICOS T cells show a young and co-stimulatory cell state and
478 are responsible for an inflammatory TME. These characteristics are recapitulated *in vitro*,
479 where these T cells signal through the PI3K and NFκB pathways, produce inflammatory

480 cytokines and do not become exhausted upon repeated tumor cell exposure. These
481 advantages were shown to be reversed when disrupting ICOS-mediated activation of PI3K.
482 Surface expression of TCR:ICOS in human T cells strictly requires a specific single amino acid
483 substitution in the intracellular tail, which does not limit antigen sensitivity nor reactivity, yet
484 preserves the TCR's ability to limit expression of the immune checkpoints PD1 and TIM3.
485 Notably, the optimized human 'ICOS cassette' was able to sustain the anti-tumor performance
486 of human T cells across multiple antigen specificities

487 TCRs that are genetically coupled to co-stimulatory molecules are conceptually similar to
488 CARs, where incorporation of a co-stimulatory molecule is standard practice. However,
489 engineering of TCRs and CARs differs significantly. In fact, TCRs face more stringent
490 structural constraints due to the complex and step-wise assembly of TCRα and TCRß chains
491 with CD3 components as well as the requirement for precise binding to peptide:MHC (39–41).
492 Consequently, most studies so far have relied on alternative concepts, such as TCRs that are
493 supported by a second chimeric co-stimulatory receptor (42), where improved T cell function
494 depends on two separate receptors. We designed and tested mouse TCRs with built-in
495 intracellular domains of either CD28, OX40 or ICOS, using, as a starting point, a chimeric TCR
496 format with the transmembrane domain of CD28 and the cytosolic domain of CD3ε (24). A
497 TCR incorporating the 4-1BB molecule did not show surface expression on mouse T cells,
498 possibly due to the tendency of murine 4-1BB to be expressed as a monomer or due to its
499 basic amino acid-rich intracellular motif that was shown to be detrimental to surface expression
500 in other settings (43–45). In fact, 4-1BB has been incorporated successfully into CARs and
501 chimeric co-receptors, but, as far we are aware, not into TCRs (42,46,47). When mice were
502 treated with TCR:OX40, TCR:CD28 and wt TCR T cells, they showed initial anti-tumor
503 responses; however, relapse of tumors ensued within 20 to 35 days, mainly resulting in no or
504 partial responses at the end of the experiments. In contrast, when mice were treated with
505 TCR:ICOS T cells, tumor relapses were delayed up to 140 days and over 40% of mice showed
506 complete responses. This anti-tumor response was accompanied by a significantly enhanced

507 persistence of TCR:ICOS-expressing CD8 T cells in the blood of mice. These findings are
508 concordant with those reported for CAR:ICOS T cells (48–51), where these T cells also
509 showed long-term persistence and a durable anti-tumor effect. Interestingly, although
510 circulating TCR:ICOS T cells were more abundant than wt TCR T cells, no difference was
511 found with respect to their phenotype. Within tumors, however, CD8 TILs that expressed
512 TCR:ICOS exhibited a less differentiated and more co-stimulatory phenotype than CD8 TILs
513 that expressed wt TCR, with close to half of the former cells harboring a naïve-like or central
514 memory state and significantly more cells expressing 4-1BB and OX40. This young, yet most
515 likely antigen-experienced and activated phenotype of TCR:ICOS T cells likely contributes to
516 the improved T cell persistence and anti-tumor response we observed in our mouse model,
517 consistent with prior reports linking less differentiated T cells to improved long-term
518 functionality (52–55). Our current flow cytometry analysis did not distinguish between naïve-
519 like and stem cell-like T cell subsets, which warrants further investigation (56). Besides, recent
520 studies have also highlighted the critical role of ICOS signaling in the formation of CD8 resident
521 memory T cells (CD8 Trm), which are recognized key players for long-term protection against
522 tumor relapse (57–59). Although we did not specifically stain for Trm markers, it is unlikely that
523 these cells were present at the time of tumor isolation since Peng and colleagues have shown
524 that CD8 Trm cells are not present yet five days after T cell transfer, and only begin to emerge
525 around days 7-8, peaking no earlier than 40 days after adoptive transfer (57). Future studies
526 could assess whether TCR:ICOS promotes Trm differentiation and investigate the kinetics of
527 these cells.

528 Treatment with TCR:ICOS T cells initiated a significant enrichment of inflammation-related
529 gene sets in regressing tumors, particularly those related to the NFκB pathway. This was
530 recapitulated *in vitro,* where antigen-stimulated TCR:ICOS T cells, but not wt TCR T cells,
531 phosphorylated multiple components of the NFκB pathway and produced significantly higher
532 levels of inflammatory cytokines that are dependent upon NFκB activation, such as CCL5, IL-
533 2, IL-6 and TNF-α (60–64). These effects were abolished in T cells expressing TCR:ICOS-YF,

534 a mutant of ICOS that does not dock nor activate PI3K, proving that activation of the NFκB
535 pathway and production of inflammatory cytokines is PI3K-dependent. Our observations,
536 particularly the ICOS-mediated increase in TNF-α secretion, extend previous reports (65,66).
537 Moreover, TNF-α was also shown to up-regulate expression of ICOS-L by antigen presenting
538 cells, thereby inducing a positive feedback loop, which may further contribute to the durable
539 responses of TCR:ICOS T cells (67). In contrast, associations between ICOS stimulation and
540 IL-2, IL-6, CCL5 and CXCL2 secretion were previously less well established (68–74).
541 Interestingly, CAR:ICOS also mediates increased antigen-specific production of TNF-α, IL-2
542 and IFN-γ compared to first-generation CARs that lack co-stimulatory molecules (49,50).
543 CAR:ICOS mediates production of IL-17 as well, a feature not observe with TCR:ICOS. This
544 discrepancy is somewhat unexpected given that both ICOS and NFκB activation have
545 previously been linked to Th17 differentiation (37,75–78). One explanation may be that CD4
546 T cell enrichments have been performed for the generation of CAR:ICOS T cells, but not
547 TCR:ICOS T cells. An alternative explanation may relate to differences in receptor affinity
548 and/or signaling since CARs bind antigen with high affinity whereas TCRs bind antigen with
549 moderate affinity and CARs are coupled to CD3ζ whereas TCRs in this study are coupled to
550 CD3ε, potentially leading to differential activation of molecules such as LAT and Lck. In
551 addition to the activation of NFκB and production of inflammatory cytokines, we also observed
552 that TCR:ICOS provided resistance to PD1 and TIM3 co-expression by T cells upon repeated
553 stimulation with antigen-positive tumor cells, again depending on PI3K. Importantly, a similar
554 observation was also made in our mouse model, where we found that mice treated with
555 TCR:ICOS-YF T cells did not demonstrate durable anti-tumor responses, underscoring the
556 critical role of PI3K-NFκB signaling in mediating the beneficial effects of TCR:ICOS T cells. It
557 is noteworthy that while CD28 also activates the PI3K and NFκB pathways, ICOS is reported
558 to more strongly recruit the p50α regulatory component of PI3K, resulting in greater
559 downstream Akt phosphorylation (79). This would indicate that the superior performance of

560 TCR:ICOS may stem from a specific sequence involving PI3K and Akt activation and
561 culminating in the engagement of NFκB (summarized in **Supplementary Figure 4e**).

562 Following determination of the therapeutic value of TCR:ICOS and identification of its
563 mechanism of action, we set out to translate TCR:ICOS to human T cells. Murine TCR:ICOS
564 (mTCR:ICOS) was expressed on the surface of human T cells, albeit at a low level, yet a fully
565 murine sequence is clinically undesirable due to its risk of inducing xenoreactivity. However,
566 the fully humanized orthologue of TCR:ICOS (hTCR:ICOS) was not expressed on the surface
567 of human T cells. Through systematic testing of 50 constructs, we identified a single amino
568 acid - arginine at position 54 in the intracellular tail of hCD3ε - as the key barrier to surface
569 expression of hTCR:ICOS. Replacing this residue with an alanine (as found in the murine
570 counterpart) completely rescued surface expression of hTCR:ICOS on human T cells. One
571 possible explanation is that the positively charged arginine in the tail of hCD3ε acts as a
572 retention signal, preventing hTCR:ICOS from exiting the endoplasmic reticulum (ER) and
573 reaching the plasma membrane. In fact, previous studies have reported that this amino acid
574 plays an integral role in an ER retention signal to guide and facilitate correct assembly of
575 TCR/CD3 components in T cells (80,81). The identification of a surface-expressed
576 hTCR:ICOS-RA variant was critical in translating this new chimeric TCR toward clinical
577 application. To expand the bandwidth of this new TCR, we also applied the optimized
578 hTCR:ICOS format to TCRs with other antigen specificities, namely NY-ESO1 and ROPN-1.
579 Once more, the R54A substitution proved both necessary and sufficient to restore surface
580 expression of hTCR:ICOS. Functional testing across all three specificities demonstrated that
581 the optimized hTCR:ICOS did not compromise antigen sensitivity nor T cell effector function.
582 This was exemplified through peptide titration assays, as well as tumor cell-specific IFN-γ
583 production and cytotoxicity, all of which were comparable to wt TCR T cells. These
584 conventional *in vitro* T cell assays have traditionally been used to guide selection of TCRs for
585 clinical development (82). However, these assays primarily measure immediate effector
586 function and may not reflect the long-term durability of T cell responses. The repeated

587 stimulation assay may serve as a valuable complementary *in vitro* tool for evaluating the
588 sustained functionality of engineered human TCRs. Importantly, the optimized hTCR:ICOS
589 did confer a clear and significant advantage in terms of resisting T cell exhaustion in this assay
590 across all TCR specificities.

591 **Conclusions**

592 In conclusion, we introduce a TCR format with built-in ICOS that enhances T cell fitness upon
593 exposure to antigen. This TCR:ICOS triggers the PI3K-NFκB pathway, drives an inflammatory
594 tumor milieu, reduces T cell exhaustion, and ultimately leads to enhanced T cell persistence
595 and long-term tumor clearance. In addition, we have developed an optimized variant of
596 TCR:ICOS that supports robust functional expression in human T cells while preserving its
597 therapeutic benefits across multiple TCR specificities. Taken together, the TCR:ICOS format
598 may constitute a promising platform for adoptive T cell therapy. In fact, preparations are
599 currently underway for a first-in-human phase 1b trial evaluating TCR:ICOS T cells targeting
600 the ROPN-1 antigen in patients with TNBC, marking a pivotal step toward clinical translation
601 and paving the way for next-generation TCR-based immunotherapies.
602

603

604 **Declarations:**

605 Ethics approval:
606 Mice experiments were approved by the Experimental Animal Committee of the Erasmus
607 MC Cancer Institute and carried out in accordance with institutional and national guidelines.
608

609 Consent for publication:
610 Not applicable.
611

612 Availability of data and materials:

The datasets used during the current study are available from the corresponding author on reasonable request.

Competing interests:

Alexandre Marraffa, Cor Berrevoets and Reno Debets report pending patent P136875EP00. Dora Hammerl reports grants from the Dutch Cancer Society and Health Holland Public-private partnership as well as pending patent P128827EP00. Rachel Abbott reports a grant from Health Holland Public-private partnership as well as support from Swanbridge Capital, Van Herk Ventures, Thuja Capital and Innovation Quarter. Reno Debets reports grants from the Erasmus MC Daniel den Hoed Foundation, the Dutch Cancer Society, Health Holland Public-private partnership and the EU, support from MSD, Bayer, and Pan Cancer T, as well as the pending patents P128827EP00 and P130556EP00. The other authors have no disclosures to report.

Funding:

This project was supported by grants from the Dutch Cancer Society (KWF 12033) and Health Holland Public-private partnership (EMCLSH 20020).

Authors' Contributions

AM: Conceptualization, data curation, formal analysis, investigation, visualization, methodology, writing and editing. **CB:** Conceptualization, data curation, investigation, methodology. **MM:** Investigation, data curation, methodology. **RW**: Investigation. **DR:** Investigation. **MvB:** Investigation. **KK:** Investigation. **M.J.W.P:** Investigation, data curation, methodology. **W.A.D:** Investigation. **AK:** data curation, investigation, methodology. **DH:** Conceptualization, writing and editing. **R.J.M.A:** funding acquisition, writing and editing. **CS:** Conceptualization, methodology, supervision, writing and editing. **RD:** Conceptualization,

methodology, resources, supervision, funding acquisition, writing and editing. All authors read and approved the final manuscript.

Acknowledgements

The authors thank Coen Govers, Rachid Bouzid, Luc Veeneman and Ana Avramovic, who participated in this work. Furthermore, we would like to thank the many healthy blood donors from Sanquin whose donation allowed the translations of our findings to the human setting.

647 **References**

648 1. Kochenderfer JN, Dudley ME, Carpenter RO, Kassim SH, Rose JJ, Telford WG, et al.
649 Donor-derived CD19-targeted T cells cause regression of malignancy persisting after allogeneic
650 hematopoietic stem cell transplantation. Blood. 2013 Dec 12;122(25):4129–39.

651 2. Brentjens RJ, Davila ML, Riviere I, Park J, Wang X, Cowell LG, et al. CD19-targeted T cells
652 rapidly induce molecular remissions in adults with chemotherapy-refractory acute
653 lymphoblastic leukemia. Sci Transl Med. 2013 Mar 20;5(177):177ra38.

654 3. Schuster SJ, Bishop MR, Tam CS, Waller EK, Borchmann P, McGuirk JP, et al.
655 Tisagenlecleucel in Adult Relapsed or Refractory Diffuse Large B-Cell Lymphoma. N Engl J Med.
656 2019 Jan 3;380(1):45–56.

657 4. Porter DL, Levine BL, Kalos M, Bagg A, June CH. Chimeric Antigen Receptor–Modified T
658 Cells in Chronic Lymphoid Leukemia. New England Journal of Medicine. 2011 Aug
659 25;365(8):725–33.

660 5. Neelapu SS, Locke FL, Bartlett NL, Lekakis LJ, Miklos DB, Jacobson CA, et al.
661 Axicabtagene Ciloleucel CAR T-Cell Therapy in Refractory Large B-Cell Lymphoma. New
662 England Journal of Medicine. 2017 Dec 28;377(26):2531–44.

663 6. Locke FL, Ghobadi A, Jacobson CA, Miklos DB, Lekakis LJ, Oluwole OO, et al. Long-term
664 safety and activity of axicabtagene ciloleucel in refractory large B-cell lymphoma (ZUMA-1): a
665 single-arm, multicentre, phase 1–2 trial. The Lancet Oncology. 2019 Jan 1;20(1):31–42.

666 7. Moretti A, Ponzo M, Nicolette CA, Tcherepanova IY, Biondi A, Magnani CF. The Past,
667 Present, and Future of Non-Viral CAR T Cells. Front Immunol. 2022;13:867013.

668 8. Sarnaik AA, Hamid O, Khushalani NI, Lewis KD, Medina T, Kluger HM, et al. Lifileucel, a
669 Tumor-Infiltrating Lymphocyte Therapy, in Metastatic Melanoma. J Clin Oncol. 2021 Aug
670 20;39(24):2656–66.

671 9. Hong DS, Van Tine BA, Biswas S, McAlpine C, Johnson ML, Olszanski AJ, et al.
672 Autologous T cell therapy for MAGE-A4+ solid cancers in HLA-A*02+ patients: a phase 1 trial.
673 Nat Med. 2023 Jan;29(1):104–14.

674 10. Kishton RJ, Restifo NP. T cells lead the charge against solid tumors. Nat Cancer. 2024
675 Dec;5(12):1762–4.

676 11. Debets R, Donnadieu E, Chouaib S, Coukos G. TCR-engineered T cells to treat tumors:
677 Seeing but not touching? Semin Immunol. 2016 Feb;28(1):10–21.

678 12. Hammerl D, Rieder D, Martens JWM, Trajanoski Z, Debets R. Adoptive T Cell Therapy:
679 New Avenues Leading to Safe Targets and Powerful Allies. Trends in Immunology. 2018 Nov
680 1;39(11):921–36.

681 13. Chandran SS, Klebanoff CA. T cell receptor-based cancer immunotherapy: Emerging
682 efficacy and pathways of resistance. Immunol Rev. 2019 Jul;290(1):127–47.

683 14. Capece D, Verzella D, Fischietti M, Zazzeroni F, Alesse E. Targeting Costimulatory
684 Molecules to Improve Antitumor Immunity. BioMed Research International.
685 2012;2012(1):926321.

686 15. Franzese O. Tumor Microenvironment Drives the Cross-Talk Between Co-Stimulatory
687 and Inhibitory Molecules in Tumor-Infiltrating Lymphocytes: Implications for Optimizing
688 Immunotherapy Outcomes. International Journal of Molecular Sciences. 2024
689 Jan;25(23):12848.

690 16. Spranger S, Spaapen RM, Zha Y, Williams J, Meng Y, Ha TT, et al. Up-Regulation of PD-
691 L1, IDO, and Tregs in the Melanoma Tumor Microenvironment Is Driven by CD8+ T Cells.
692 Science Translational Medicine. 2013 Aug 28;5(200):200ra116-200ra116.

693 17. Gyurdieva A, Zajic S, Chang YF, Houseman EA, Zhong S, Kim J, et al. Biomarker
694 correlates with response to NY-ESO-1 TCR T cells in patients with synovial sarcoma. Nat
695 Commun. 2022 Sep 8;13(1):5296.

696 18. Galon J, Costes A, Sanchez-Cabo F, Kirilovsky A, Mlecnik B, Lagorce-Pagès C, et al.
697 Type, Density, and Location of Immune Cells Within Human Colorectal Tumors Predict Clinical
698 Outcome. Science. 2006 Sep 29;313(5795):1960–4.

699 19. Hammerl D, Martens JWM, Timmermans M, Smid M, Trapman-Jansen AM, Foekens R, et
700 al. Spatial immunophenotypes predict response to anti-PD1 treatment and capture distinct
701 paths of T cell evasion in triple negative breast cancer. Nat Commun. 2021 Sep 27;12(1):5668.

702 20. Schaft N, Willemsen RA, de Vries J, Lankiewicz B, Essers BWL, Gratama JW, et al.
703 Peptide fine specificity of anti-glycoprotein 100 CTL is preserved following transfer of
704 engineered TCR alpha beta genes into primary human T lymphocytes. J Immunol. 2003 Feb
705 15;170(4):2186–94.

706 21. Pouw NMC, Westerlaken EJ, Willemsen RA, Debets R. Gene transfer of human TCR in
707 primary murine T cells is improved by pseudo-typing with amphotropic and ecotropic
708 envelopes. J Gene Med. 2007 Jul;9(7):561–70.

709 22. Engels B, Cam H, Schüler T, Indraccolo S, Gladow M, Baum C, et al. Retroviral vectors
710 for high-level transgene expression in T lymphocytes. Hum Gene Ther. 2003 Aug
711 10;14(12):1155–68.

712 23. Straetemans T, Berrevoets C, Coccoris M, Treffers-Westerlaken E, Wijers R, Cole DK, et
713 al. Recurrence of Melanoma Following T Cell Treatment: Continued Antigen Expression in a
714 Tumor That Evades T Cell Recruitment. Mol Ther. 2015 Feb;23(2):396–406.

715 24. Govers C, Sebestyén Z, Roszik J, van Brakel M, Berrevoets C, Szöőr Á, et al. TCRs
716 genetically linked to CD28 and CD3ε do not mispair with endogenous TCR chains and mediate

717 enhanced T cell persistence and anti-melanoma activity. J Immunol. 2014 Nov
718 15;193(10):5315–26.

719 25. Gigoux M, Shang J, Pak Y, Xu M, Choe J, Mak TW, et al. Inducible costimulator promotes
720 helper T-cell differentiation through phosphoinositide 3-kinase. Proc Natl Acad Sci U S A. 2009
721 Dec 1;106(48):20371–6.

722 26. D'Angelo SP, Melchiori L, Merchant MS, Bernstein D, Glod J, Kaplan R, et al. Antitumor
723 Activity Associated with Prolonged Persistence of Adoptively Transferred NY-ESO-1 c259T Cells
724 in Synovial Sarcoma. Cancer Discov. 2018 Aug;8(8):944–57.

725 27. Kortleve D, Hammerl D, van Brakel M, Wijers R, Roelofs D, Kroese K, et al. TCR-
726 engineered T-cells directed against Ropporin-1 constitute a safe and effective treatment for
727 triple-negative breast cancer. Cancer Discov. 2024 Aug 22;

728 28. Li Y, Moysey R, Molloy PE, Vuidepot AL, Mahon T, Baston E, et al. Directed evolution of
729 human T-cell receptors with picomolar affinities by phage display. Nat Biotechnol. 2005
730 Mar;23(3):349–54.

731 29. Soneoka Y, Cannon PM, Ramsdale EE, Griffiths JC, Romano G, Kingsman SM, et al. A
732 transient three-plasmid expression system for the production of high titer retroviral vectors.
733 Nucleic Acids Res. 1995 Feb 25;23(4):628–33.

734 30. Lamers CHJ, Willemsen RA, Luider BA, Debets R, Bolhuis RLH. Protocol for gene
735 transduction and expansion of human T lymphocytes for clinical immunogene therapy of
736 cancer. Cancer Gene Ther. 2002 Jul;9(7):613–23.

737 31. Weijtens ME, Willemsen RA, Hart EH, Bolhuis RL. A retroviral vector system 'STITCH' in
738 combination with an optimized single chain antibody chimeric receptor gene structure allows
739 efficient gene transduction and expression in human T lymphocytes. Gene Ther. 1998
740 Sep;5(9):1195–203.

741 32. Lamers CHJ, van Steenbergen-Langeveld S, van Brakel M, Groot-van Ruijven CM, van
742 Elzakker PMML, van Krimpen B, et al. T Cell Receptor-Engineered T Cells to Treat Solid Tumors:
743 T Cell Processing Toward Optimal T Cell Fitness. Hum Gene Ther Methods. 2014 Dec
744 1;25(6):345–57.

745 33. Pascolo S, Bervas N, Ure JM, Smith AG, Lemonnier FA, Pérarnau B. HLA-A2.1-restricted
746 education and cytolytic activity of CD8(+) T lymphocytes from beta2 microglobulin (beta2m)
747 HLA-A2.1 monochain transgenic H-2Db beta2m double knockout mice. J Exp Med. 1997 Jun
748 16;185(12):2043–51.

749 34. Seynhaeve ALB, Hoving S, Schipper D, Vermeulen CE, de Wiel-Ambagtsheer G aan, van
750 Tiel ST, et al. Tumor necrosis factor alpha mediates homogeneous distribution of liposomes in
751 murine melanoma that contributes to a better tumor response. Cancer Res. 2007 Oct
752 1;67(19):9455–62.

753 35. Hammerl D, Massink MPG, Smid M, van Deurzen CHM, Meijers-Heijboer HEJ, Waisfisz
754 Q, et al. Clonality, Antigen Recognition, and Suppression of CD8+ T Cells Differentially Affect
755 Prognosis of Breast Cancer Subtypes. Clin Cancer Res. 2020 Jan 15;26(2):505–17.

756 36. Kortleve D, Coelho RML, Hammerl D, Debets R. Cancer germline antigens and tumor-
757 agnostic CD8+ T cell evasion. Trends Immunol. 2022 May;43(5):391–403.

758 37. Liu T, Zhang L, Joo D, Sun SC. NF-κB signaling in inflammation. Signal Transduct Target
759 Ther. 2017 Jul 14;2:17023.

760 38. Su CM, Wang L, Yoo D. Activation of NF-κB and induction of proinflammatory cytokine
761 expressions mediated by ORF7a protein of SARS-CoV-2. Sci Rep. 2021 Jun 29;11(1):13464.

762 39. Geisler C, Kuhlmann J, Rubin B. Assembly, intracellular processing, and expression at
763 the cell surface of the human alpha beta T cell receptor/CD3 complex. Function of the CD3-
764 zeta chain. Journal of Immunology. 1989;143(12):4069–77.

765 40. Kappes DJ, Tonegawa S. Surface expression of alternative forms of the TCR/CD3
766 complex. Proceedings of the National Academy of Sciences. 1991 Dec;88(23):10619–23.

767 41. Hall C, Berkhout B, Alarcon B, Sancho J, Wileman T, Terhorst C. Requirements for cell
768 surface expression of the human TCR/CD3 complex in non-T cells. Int Immunol. 1991
769 Apr;3(4):359–68.

770 42. Hernández-López P, van Diest E, Brazda P, Heijhuurs S, Meringa A, Hoorens van
771 Heyningen L, et al. Dual targeting of cancer metabolome and stress antigens affects
772 transcriptomic heterogeneity and efficacy of engineered T cells. Nat Immunol. 2024
773 Jan;25(1):88–101.

774 43. Lah S, Kim S, Kang I, Kim H, Hupperetz C, Jung H, et al. Engineering second-generation
775 TCR-T cells by site-specific integration of TRAF-binding motifs into the CD247 locus. J
776 Immunother Cancer. 2023 Apr 1;11(4):e005519.

777 44. Chin SM, Kimberlin CR, Roe-Zurz Z, Zhang P, Xu A, Liao-Chan S, et al. Structure of the 4-
778 1BB/4-1BBL complex and distinct binding and functional properties of utomilumab and
779 urelumab. Nat Commun. 2018 Nov 8;9(1):4679.

780 45. Bitra A, Doukov T, Destito G, Croft M, Zajonc DM. Crystal structure of the m4-1BB/4-
781 1BBL complex reveals an unusual dimeric ligand that undergoes structural changes upon 4-
782 1BB receptor binding. J Biol Chem. 2019 Feb 8;294(6):1831–45.

783 46. Milone MC, Fish JD, Carpenito C, Carroll RG, Binder GK, Teachey D, et al. Chimeric
784 receptors containing CD137 signal transduction domains mediate enhanced survival of T cells
785 and increased antileukemic efficacy in vivo. Mol Ther. 2009 Aug;17(8):1453–64.

786 47. Zhi L, Yin M, Su X, Zhang Z, Lu H, Li M, et al. A chimeric switch-receptor PD1-DAP10-
787 41BB augments NK92-cell activation and killing for human lung Cancer H1299 Cell.
788 Biochemical and Biophysical Research Communications. 2022 Apr 16;600:94–100.

789 48. Shen CJ, Yang YX, Han EQ, Cao N, Wang YF, Wang Y, et al. Chimeric antigen receptor
790 containing ICOS signaling domain mediates specific and efficient antitumor effect of T cells
791 against EGFRvIII expressing glioma. Journal of Hematology & Oncology. 2013 May 9;6(1):33.

792 49. Guedan S, Chen X, Madar A, Carpenito C, McGettigan SE, Frigault MJ, et al. ICOS-based
793 chimeric antigen receptors program bipolar TH17/TH1 cells. Blood. 2014 Aug 14;124(7):1070–
794 80.

795 50. Guedan S, Posey AD, Shaw C, Wing A, Da T, Patel PR, et al. Enhancing CAR T cell
796 persistence through ICOS and 4-1BB costimulation. JCI Insight. 2018 Jan 11;3(1):e96976,
797 96976.

798 51. Guedan S, Madar A, Casado-Medrano V, Shaw C, Wing A, Liu F, et al. Single residue in
799 CD28-costimulated CAR-T cells limits long-term persistence and antitumor durability. 2020 Jun
800 1;

801 52. Tantalo DG, Oliver AJ, von Scheidt B, Harrison AJ, Mueller SN, Kershaw MH, et al.
802 Understanding T cell phenotype for the design of effective chimeric antigen receptor T cell
803 therapies. J Immunother Cancer. 2021 May 25;9(5):e002555.

804 53. Klebanoff CA, Gattinoni L, Palmer DC, Muranski P, Ji Y, Hinrichs CS, et al. Determinants
805 of Successful CD8+ T-Cell Adoptive Immunotherapy for Large Established Tumors in Mice.
806 Clinical Cancer Research. 2011 Aug 14;17(16):5343–52.

807 54. Kwon BS, Weissman SM. cDNA sequences of two inducible T-cell genes. Proc Natl Acad
808 Sci U S A. 1989 Mar;86(6):1963–7.

809 55. Fujita T, Ukyo N, Hori T, Uchiyama T. Functional characterization of OX40 expressed on
810 human CD8+ T cells. Immunology Letters. 2006 Jul 15;106(1):27–33.

811 56. Gattinoni L, Klebanoff CA, Restifo NP. Paths to stemness: building the ultimate
812 antitumour T cell. Nat Rev Cancer. 2012 Oct;12(10):671–84.

813 57. Peng C, Huggins MA, Wanhainen KM, Knutson TP, Lu H, Georgiev H, et al. Engagement
814 of the costimulatory molecule ICOS in tissues promotes establishment of CD8+ tissue-resident
815 memory T cells. Immunity. 2022 Jan 11;55(1):98-114.e5.

816 58. Damei I, Trickovic T, Mami-Chouaib F, Corgnac S. Tumor-resident memory T cells as a
817 biomarker of the response to cancer immunotherapy. Front Immunol. 2023 Jul 20;14.

818 59. Okła K, Farber DL, Zou W. Tissue-resident memory T cells in tumor immunity and
819 immunotherapy. J Exp Med. 2021 Apr 5;218(4):e20201605.

820 60. Takeuchi O, Akira S. Pattern Recognition Receptors and Inflammation. Cell. 2010 Mar
821 19;140(6):805–20.

822 61. Wickremasinghe MI, Thomas LH, O'Kane CM, Uddin J, Friedland JS. Transcriptional
823 mechanisms regulating alveolar epithelial cell-specific CCL5 secretion in pulmonary
824 tuberculosis. J Biol Chem. 2004 Jun 25;279(26):27199–210.

825 62. Hoyos B, Ballard DW, Böhnlein E, Siekevitz M, Greene WC. Kappa B-specific DNA
826 binding proteins: role in the regulation of human interleukin-2 gene expression. Science. 1989
827 Apr 28;244(4903):457–60.

828 63. Libermann TA, Baltimore D. Activation of interleukin-6 gene expression through the NF-
829 kappa B transcription factor. Mol Cell Biol. 1990 May;10(5):2327–34.

830 64. Collart MA, Baeuerle P, Vassalli P. Regulation of tumor necrosis factor alpha
831 transcription in macrophages: involvement of four kappa B-like motifs and of constitutive and
832 inducible forms of NF-kappa B. Mol Cell Biol. 1990 Apr;10(4):1498–506.

833 65. Li J, Heinrichs J, Leconte J, Haarberg K, Semple K, Liu C, et al. Phosphatidylinositol 3-
834 Kinase–Independent Signaling Pathways Contribute to ICOS-Mediated T Cell Costimulation in
835 Acute Graft-Versus-Host Disease in Mice. J Immunol. 2013 Jul 1;191(1):200–7.

836 66. Sainson RCA, Thotakura AK, Kosmac M, Borhis G, Parveen N, Kimber R, et al. An
837 Antibody Targeting ICOS Increases Intratumoral Cytotoxic to Regulatory T-cell Ratio and
838 Induces Tumor Regression. Cancer Immunol Res. 2020 Dec;8(12):1568–82.

839 67. Richter G, Hayden-Ledbetter M, Irgang M, Ledbetter JA, Westermann J, Körner I, et al.
840 Tumor Necrosis Factor-α Regulates the Expression of Inducible Costimulator Receptor Ligand
841 on CD34+ Progenitor Cells during Differentiation into Antigen Presenting Cells*. Journal of
842 Biological Chemistry. 2001 Dec 7;276(49):45686–93.

843 68. Odegard JM, DiPlacido LD, Greenwald L, Kashgarian M, Kono DH, Dong C, et al. ICOS
844 Controls Effector Function but Not Trafficking Receptor Expression of Kidney-Infiltrating
845 Effector T Cells in Murine Lupus. J Immunol. 2009 Apr 1;182(7):4076–84.

846 69. Alves GF, Stoppa I, Aimaretti E, Monge C, Mastrocola R, Porchietto E, et al. ICOS-Fc as
847 innovative immunomodulatory approach to counteract inflammation and organ injury in sepsis.
848 Front Immunol. 2022 Sep 2;13.

849 70. Riley JL, Blair PJ, Musser JT, Abe R, Tezuka K, Tsuji T, et al. ICOS Costimulation Requires
850 IL-2 and Can Be Prevented by CTLA-4 Engagement1. The Journal of Immunology. 2001 Apr
851 15;166(8):4943–8.

852 71. Harada Y, Ohgai D, Watanabe R, Okano K, Koiwai O, Tanabe K, et al. A single amino acid
853 alteration in cytoplasmic domain determines IL-2 promoter activation by ligation of CD28 but
854 not inducible costimulator (ICOS). J Exp Med. 2003 Jan 20;197(2):257–62.

855 72. Hutloff A, Dittrich AM, Beier KC, Eljaschewitsch B, Kraft R, Anagnostopoulos I, et al.
856 ICOS is an inducible T-cell co-stimulator structurally and functionally related to CD28. Nature.
857 1999 Dec;402(6763):21–4.

858 73. Yoshinaga SK, Zhang M, Pistillo J, Horan T, Khare SD, Miner K, et al. Characterization of a
859 new human B7-related protein: B7RP-1 is the ligand to the co-stimulatory protein ICOS. Int
860 Immunol. 2000 Oct;12(10):1439–47.

861 74. Yoshinaga SK, Whoriskey JS, Khare SD, Sarmiento U, Guo J, Horan T, et al. T-cell co-
862 stimulation through B7RP-1 and ICOS. Nature. 1999 Dec;402(6763):827–32.

863 75. Park SH, Cho G, Park SG. NF-κB Activation in T Helper 17 Cell Differentiation. Immune
864 Netw. 2014 Feb;14(1):14–20.

865 76. Molinero LL, Cubre A, Mora-Solano C, Wang Y, Alegre ML. T cell receptor/CARMA1/NF-
866 κB signaling controls T-helper (Th) 17 differentiation. Proceedings of the National Academy of
867 Sciences. 2012 Nov 6;109(45):18529–34.

868 77. Wyatt MM, Huff LW, Nelson MH, Neal LR, Medvec AR, Rangel Rivera GO, et al.
869 Augmenting TCR signal strength and ICOS costimulation results in metabolically fit and
870 therapeutically potent human CAR Th17 cells. Mol Ther. 2023 Jul 5;31(7):2120–31.

871 78. Paulos CM, Carpenito C, Plesa G, Suhoski MM, Varela-Rohena A, Golovina TN, et al. The
872 inducible costimulator (ICOS) is critical for the development of human T(H)17 cells. Sci Transl
873 Med. 2010 Oct 27;2(55):55ra78.

874 79. Fos C, Salles A, Lang V, Carrette F, Audebert S, Pastor S, et al. ICOS ligation recruits the
875 p50alpha PI3K regulatory subunit to the immunological synapse. J Immunol. 2008 Aug
876 1;181(3):1969–77.

877 80. Delgado P, Alarcón B. An orderly inactivation of intracellular retention signals controls
878 surface expression of the T cell antigen receptor. J Exp Med. 2005 Feb 21;201(4):555–66.

879 81. Schutze MP, Peterson PA, Jackson MR. An N-terminal double-arginine motif maintains
880 type II membrane proteins in the endoplasmic reticulum. The EMBO Journal. 1994 Apr
881 1;13(7):1696.

882 82. Kortleve D, Brakel M van, Wijers R, Debets R, Hammerl D. Gene Engineering T Cells with
883 T-Cell Receptor for Adoptive Therapy. In: Immunogenetics: Methods and Protocols [Internet].
884 Humana; 2022.

885 **List of abbreviations:**

886 **CAR :** chimeric antigen receptor

887 **CD:** cluster of differentiation

888 **CCL:** Chemokine (C-C motif) ligand

889 **CMM :** Complete mouse medium

890 **CXCL:** Chemokine (C-X-C motif)

891 **DNA :** Deoxyribonucleic acid

892 **EC:** Extracellular

893 **ER:** Endoplasmic reticulum

894 **ELISA:** Enzyme linked immunosorbent assay

895 **FDA:** Food and drug administration

896 **GFP:** Green fluorescent protein

897 **HLA:** Human leukocyte antigen

898 **IC:** Intracellular

899 **ICOS:** Inducible T cell co-stimulator

900 **IFN-γ:** Interferon gamma

901 **IL**: Interleukin

902 **IKK:** IkappaB-kinase

903 **MHC:** Major histocompatibility complex

904 **MMP:** matrix metalloproteinase

905 **NF-κB :** Nuclear factor kappa B

906 **NY-ESO1:** New-York esophageal squamous cell carcinoma 1

907 **PBMC:** peripheral blood mononuclear cell

908 **PCR:** Polymerase chain reaction

909 **PD1:** programmed cell death protein 1

910 **PI3K:** Phosphoinositide 3-kinase

911 **RNA:** Ribonucleic acid

912 **ROPN1:** Rhophilin associated tail protein 1

913 **RT:** Room temperature

914 **TCR:** T cell receptor

915 **Th17:** T helper 17

916 **TIL:** Tumor infiltrating lymphocyte

917 **TIM3:** T cell immunoglobulin mucin-3

918 **TM:** Transmembrane

919 **TME:** Tumor micro-environment

920 **TNBC:** Triple negative breast cancer

921 **TNF-α:** Tumor necrosis factor alpha

922 **Trm:** Tissue resident memory (T cell)

923 **wt:** Wildtype

924

Figure 1

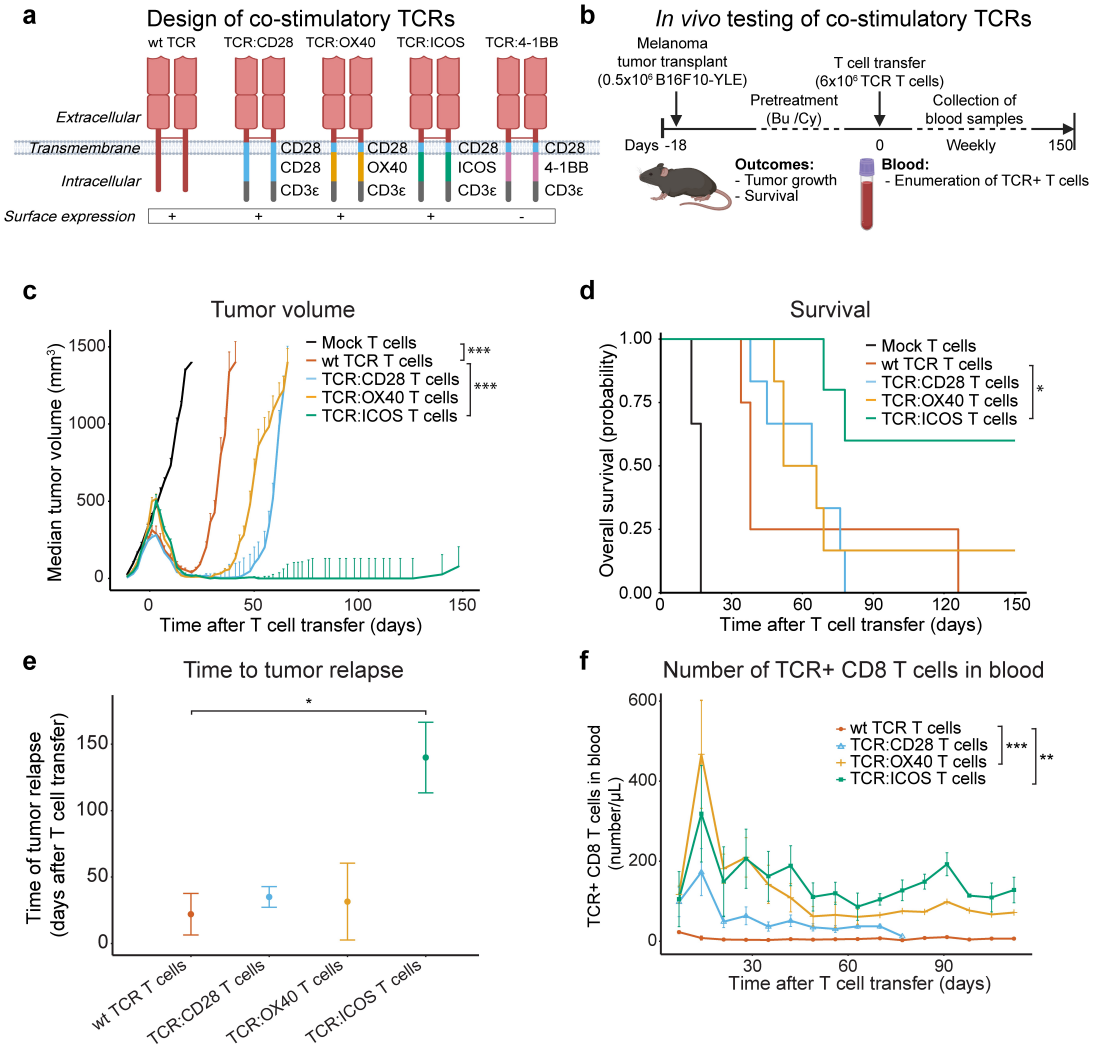

Figure 1. *TCR:ICOS mediates durable anti-melanoma T cell responses.* **(a)** Schematic illustration of the design of murine co-stimulatory TCRs, where extracellular TCR-VαCα and VßCß chains targeting human gp100/A2 were coupled to the murine transmembrane domain of CD28, followed by the murine intracellular domains of either CD28, OX40, ICOS or 4-1BB, and the intracellular domain of CD3ε. **(b)** C57BL/6 HHD mice were transplanted with B16:HHD-YLE cells expressing the HLA-A2-restricted gp100 epitope YLEPGPVTA. Prior to adoptive T cell transfer on day 0, mice received busulfan and cyclophosphamide, after which mice were administered $6x10^6$ mock, wt TCR, TCR:CD28, TCR:OX40 or TCR:ICOS T cells. Mice were then monitored for 150 days after T cell transfer for tumor volume, survival and

935 number of TCR T cells in blood. **(c)** Tumor volume, displayed in mm^3 following T cell transfer
936 (median+SEM, n=4-6 per group). Mice attaining a tumor volume>1400 mm^3 were sacrificed.
937 Statistical testing between groups was performed with linear mixed model with elapsed time
938 as a separate variable and correction for random effect. Significant interactions between time
939 and treatment on tumor volume is displayed. **(d)** Survival of mice showing initial response
940 following T cell transfer is plotted as Kaplan-Meier curves. Statistical inter-group comparison
941 was done according to Cox regression. **(e)** Time to tumor relapse in days following T cell
942 transfer is plotted (median±SEM, n=4-6). Inter-group comparison was done according to
943 Kruskal-Wallis testing, with post-hoc Dunn's test. **(f)** Numbers of TCR+ CD8 T cells per µL
944 blood following T cell transfer are displayed as determined by flow cytometry (median±SEM,
945 n=4-6). Inter-group comparison was done according to linear mixed model with elapsed time
946 as a separate variable and correction for random effect. With * = $p<0.05$, ** = $p<0.01$, *** =
947 $p<0.001$.

Figure 2

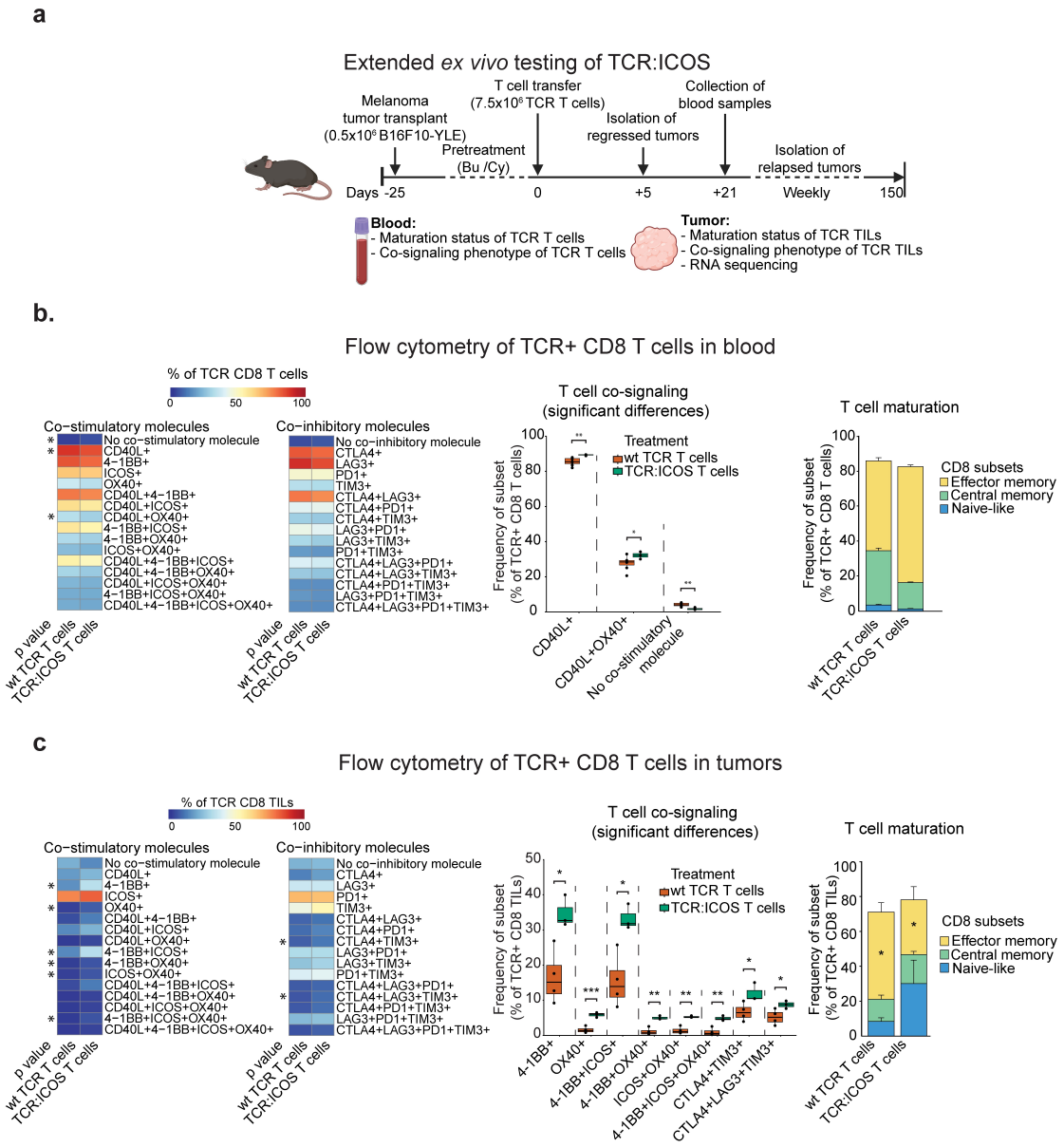

Figure 2. *Intra-tumoral TCR:ICOS CD8 T cells exhibit a young and co-stimulatory phenotype.* **(a)** Experimental design, in which C57BL/6 HHD mice were transplanted with B16:HHD-YLE melanoma cells on day -25 and pre-treated with busulfan and cyclophosphamide, after which mice were administered 7.5x10^6 wt TCR or TCR:ICOS T cells on day 0. Monitoring included frequency assessment of subsets of TCR+ CD8 T cells in blood (at three weeks after T cell transfer) and TILs (in regressing tumors at five days after T cell transfer) according to maturation and co-signaling status as well as transcriptomics of tumors **(b)** Left panel:

956 heatmap corresponding to phenotype of TCR+ CD8 T cells in blood as determined by flow
957 cytometry. Co-signaling phenotype of T cells was determined according to the expression of
958 (combinations of) co-inhibitory (CTLA4, LAG3, PD1, TIM3) or co-stimulatory receptors
959 (CD40L, 4-1BB, ICOS, OX40). The heatmap displays median expressions of single or multiple
960 markers, n=3-8 per group. Statistical significance between TCR:ICOS and wt TCR T cells was
961 assessed according to t-test and is highlighted at left-hand side. Middle panel: TCR:ICOS+
962 CD8 T cell subsets that show differential frequencies when compared to wt TCR+ CD8 T cells.
963 Right panel: stacked bars corresponding to maturation phenotype of TCR+ CD8 T cells in
964 blood as determined by flow cytometry (n=3-8 per group). Maturation status of T cells was
965 defined as follows: naïve-like T cells, CD62L+CD44-; central memory T cells, CD62L+CD44+;
966 and effector memory T cells, CD62L-CD44+. Statistical significance between TCR:ICOS and
967 wt TCR T cells was assessed according to Kruskal-Wallis testing. **(c)** Left and right panels:
968 heatmap and stacked bars corresponding to phenotype of TCR+ CD8 TILs from regressing
969 tumors as determined by flow cytometry. Middle panel: TCR:ICOS+ CD8 TIL subsets that
970 show differential frequencies when compared to wt TCR+ CD8 TILs (n=2-4 per group). With *
971 = $p<0.05$, ** = $p<0.01$, *** = $p<0.001$.

Figure 3

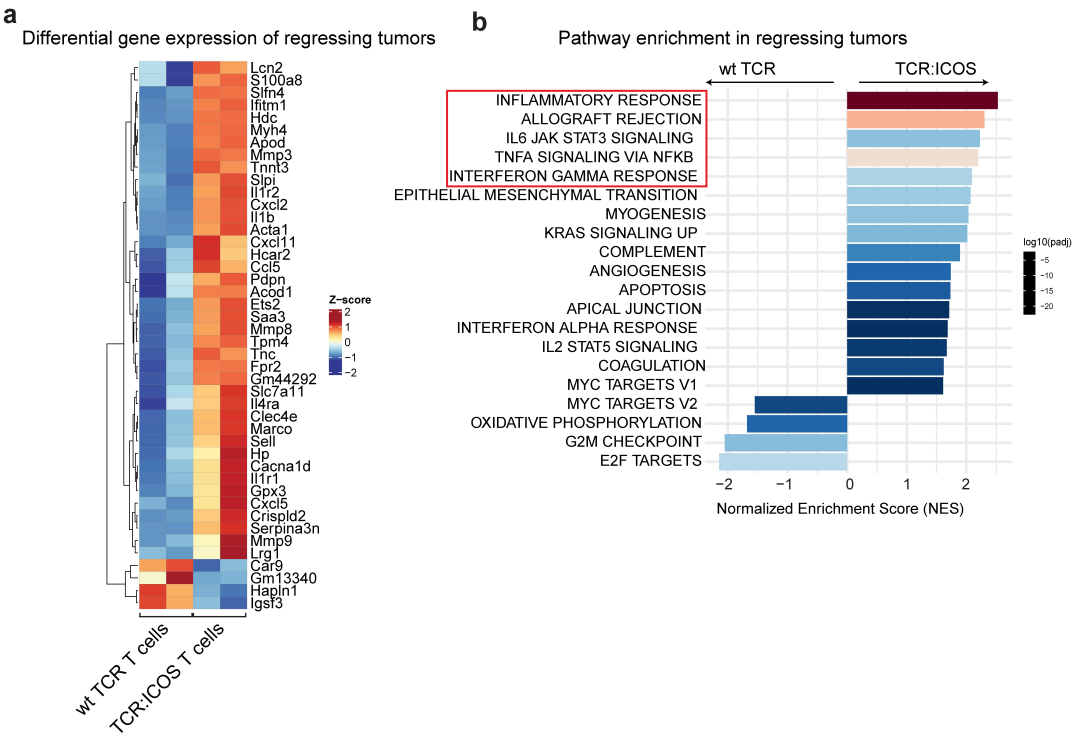

Figure 3. *TCR:ICOS T cells create an inflammatory micro-environment in tumors.* Regressing tumor tissues from mice treated with wt TCR T cells or TCR:ICOS T cells were isolated on day five for transcriptomic analysis. **(a)** Heatmap displaying all genes with an absolute log2FC >2, a base mean >50 and an adjusted p-value<0.05 for TCR:ICOS T cells when compared to wt TCR T cells (n=2 per group). **(b)** Bar graph showing top 20 gene sets that are differentially enriched following transfer of TCR:ICOS T cells or wt TCR T cells.

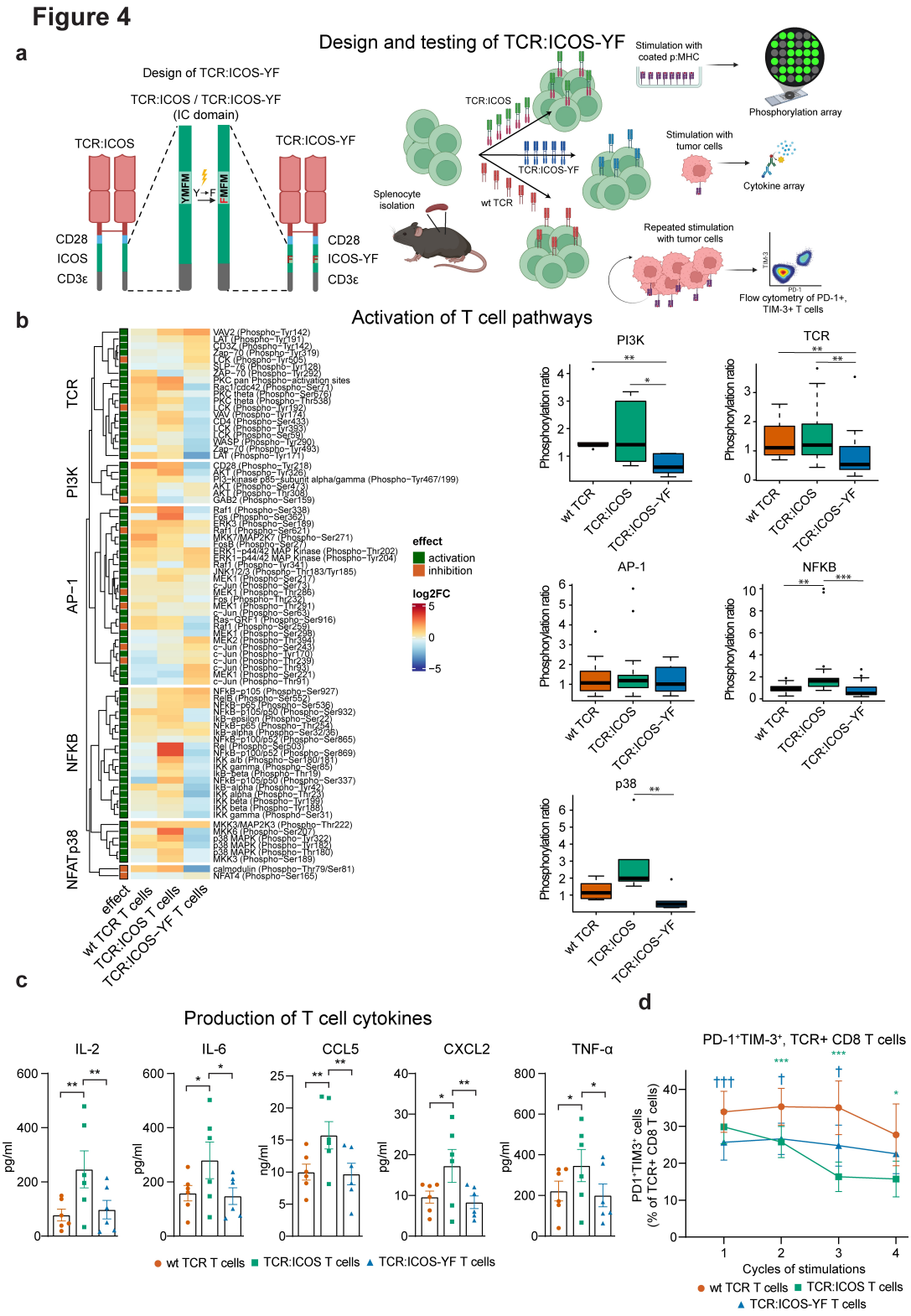

Figure 4. *In vitro stimulated TCR:ICOS T cells activate the NFκB pathway, produce inflammatory cytokines and are resistant to exhaustion upon repeated tumor cell exposure.*

982 **(a)** Left panel: graphical representation of TCR:ICOS-YF, where the intracellular ICOS domain
983 is mutated at a single site to prevent docking of PI3K and downstream signaling. Right panel:
984 experimental design in which mouse splenocytes that express either TCR:ICOS, TCR:ICOS-
985 YF or wt TCR were interrogated for intracellular signaling, cytokine production and ability to
986 preserve fitness upon repeated antigen stimulation. **(b)** Left panel: heatmap corresponding to
987 fold-change in protein phosphorylation in wt TCR, TCR:ICOS and TCR:ICOS-YF T cells upon
988 stimulation. Mouse T cells were incubated for 30 min at 37°C with pre-coated A2Kb pentamers
989 presenting the cognate epitope, after which cells were lysed and lysates were exposed to a
990 fluorescence-based phosphorylation array covering more than 70 substrates representing T
991 cell signaling. In the heatmap, phosphorylated targets were categorized according to different
992 intracellular pathways. The effect of phosphorylation on a particular pathway is displayed to
993 the left, with red representing an inhibitory and green an activating substrate. Right panel: box
994 plots displaying ratio of phosphorylated substrates associated with different pathways, only
995 taking into account pathway-activating substrates. Comparison between groups was
996 performed using a Kruskal-Wallis, followed by post-hoc Dunn's test. **(c)** Bar graphs displaying
997 cytokine production of TCR T cells following stimulation with tumor cells. T cells were
998 incubated for 16h at 37°C with B16 cells that expressed the cognate epitope, after which
999 supernatants were assayed for the presence of 14 cytokines according to a cytokine bead
1000 array. Statistical significance between groups was tested with two-way ANOVAs with Dunnet's
1001 multiple comparison test. Only the conditions in which significant differences were observed
1002 are displayed here, with the full panel of cytokines being available in **Supplementary Figure**
1003 **4c. (d)** Average percentages of $PD1^{+}TIM3^{+}$ TCR+ CD8 T cells following repeated stimulations
1004 (±SEM, n=9). Co-culture with B16F10 wt tumor cells not expressing the cognate epitope did
1005 not result in changed percentages of this T cell subset and was used to normalize the
1006 background expression. Statistical significance between groups was tested with a mixed
1007 model analysis, and post-hoc analysis per cycle was performed with Dunnet's multiple
1008 comparison test. Statistical significance between TCR:ICOS and wt TCR T cells is depicted

with a star (*), and between TCR:ICOS-YF and wt TCR with a cross (†). With * = p<0.05, ** = p<0.01, *** = p<0.001.

Figure 5

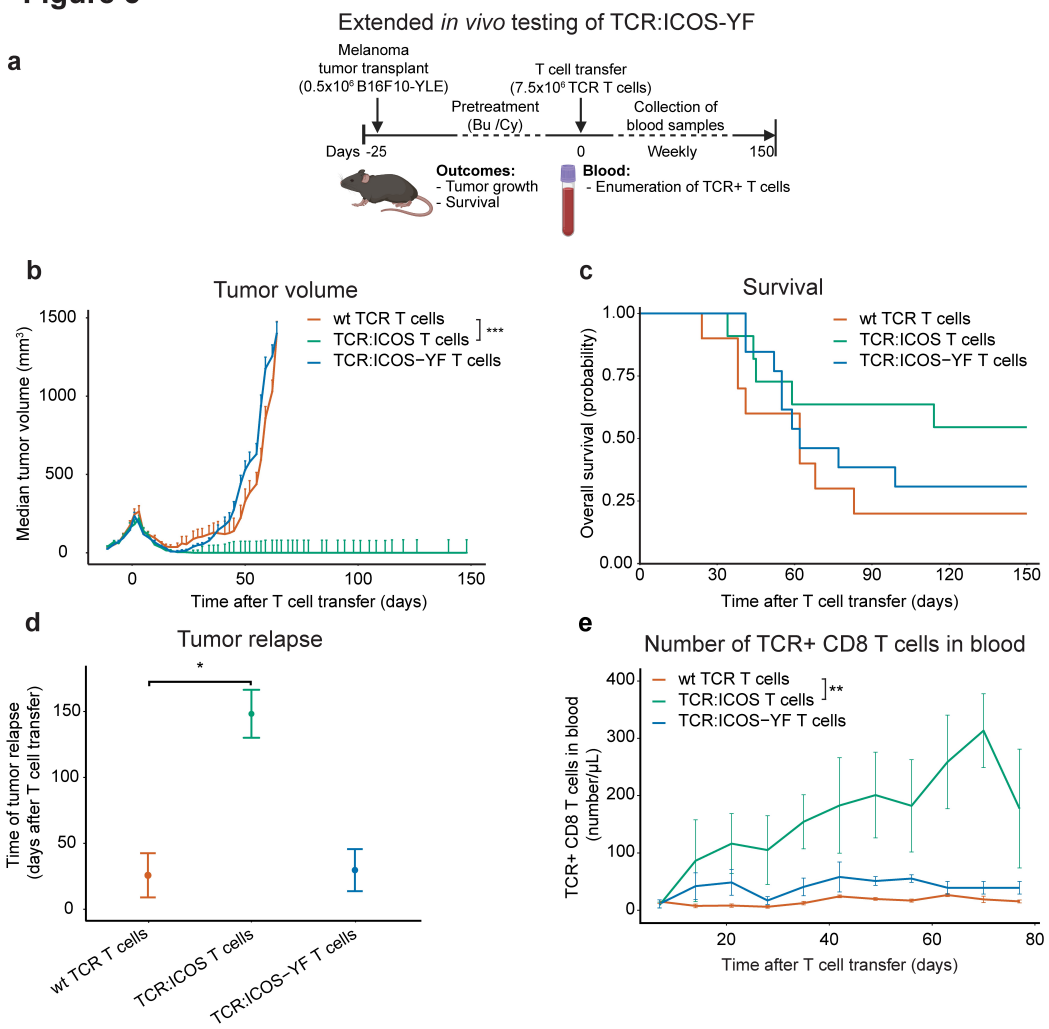

Figure 5. *Durability of anti-tumor response of T cells depends on ICOS docking site for PI3K.* **(a)** TCR:ICOS-YF T cells were studied for their *in vivo* anti-tumor performance. Schematic illustration of experimental design, in which mice were transplanted with B16:HHD-YLE melanoma cells and pre-treated with chemotherapy, after which mice were administered $7.5x10^6$ wt TCR, TCR:ICOS or TCR:ICOS-YF T cells. Monitoring included tumor growth and assessment of subsets of TCR+ CD8 T cells in blood. **(b)** Line graph displaying tumor volume in mm^3 following T cell transfer (median+SEM, n=10-13 per group, pooled from 2 independent

1019 experiments). Statistical testing between groups was performed with linear mixed model with
1020 elapsed time as a separate variable and correction for random effect. Significant interaction
1021 between time and treatment on tumor volume is displayed. **(c)** Survival of mice following initial
1022 response to T cell transfer is plotted as Kaplan-Meier curves. **(d)** Time to tumor relapse in
1023 days following T cell transfer is plotted (median±SEM, n=10-13, pooled from 2 independent
1024 experiments). Inter-group comparison was performed using a Kruskal-Wallis test. **(e)** Number
1025 of TCR+ CD8 T cells per μL blood following T cell transfer is plotted as determined by flow
1026 cytometry (median±SEM, n=10-13, pooled from 2 independent experiments. Statistical testing
1027 between groups was performed with linear mixed model with elapsed time as a separate
1028 variable and correction for random effect. Significant interaction between time and treatment
1029 on T cell number is displayed. With * = $p<0.05$, ** = $p<0.01$, *** = $p<0.001$.

Figure 6

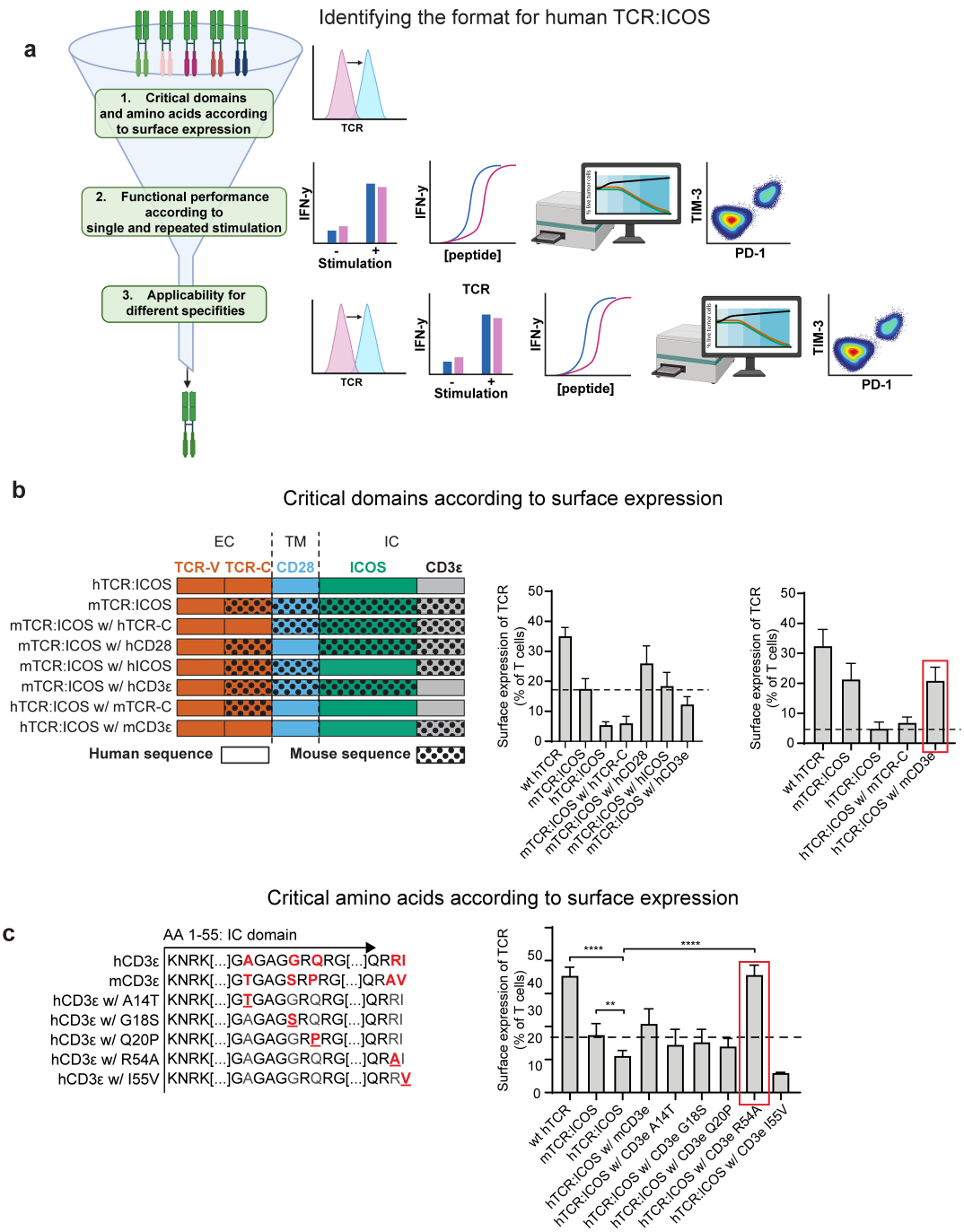

1030

Figure 6 continued

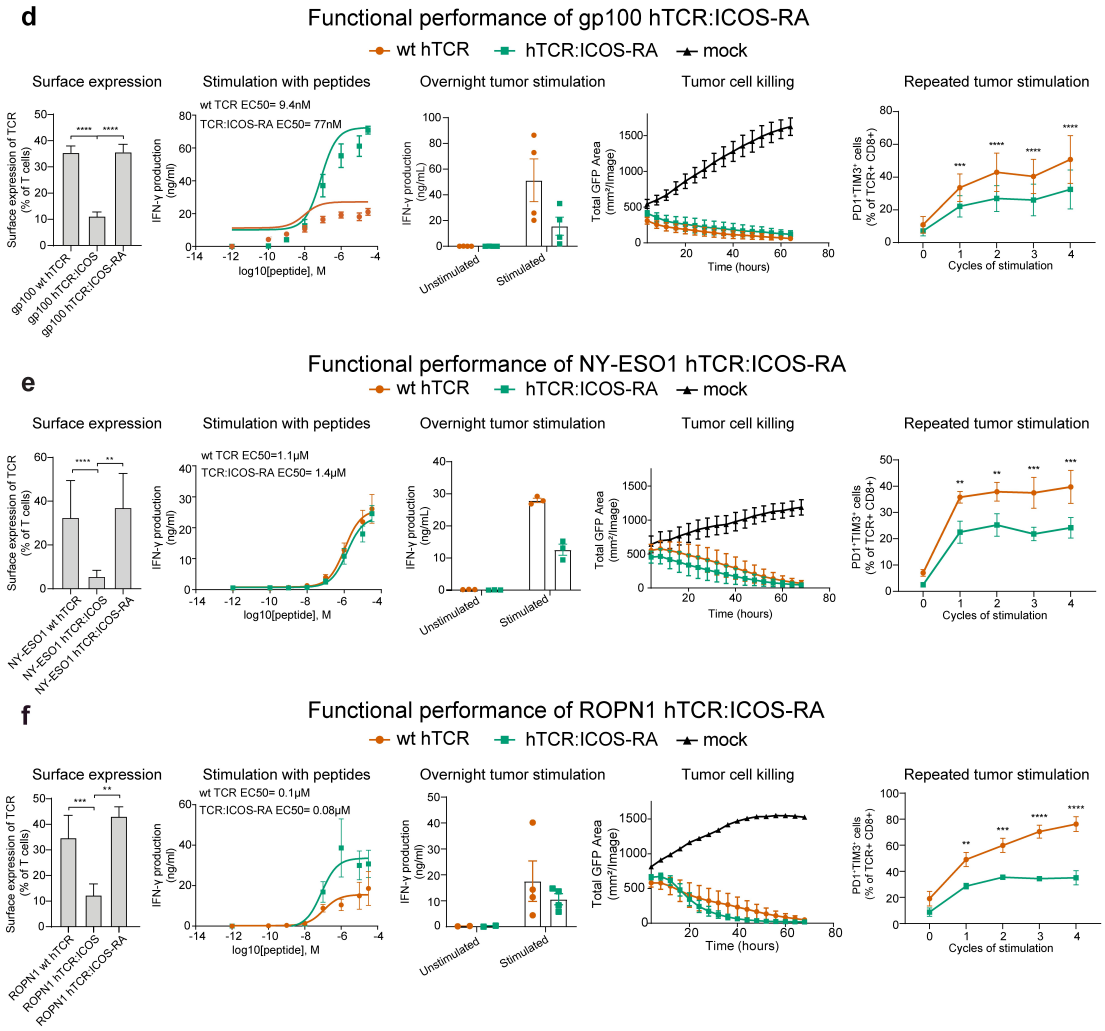

Figure 6. *A single amino acid substitution in the cytosolic tail of the CD3ε domain enables functional expression of TCR:ICOS in human T cells.* **(a)** Schematic illustration of the selection and testing strategy of hTCR:ICOS variants. **(b)** Identification of single building blocks that are required for surface expression of mTCR:ICOS. Left panel: cartoon of the first series of mouse (m) / human (h) TCR:ICOS variants, with mouse sequences highlighted by black dots. Right panels: surface expression of m/h TCR:ICOS variants according to % TCR-Vß14 of TCR T cells corrected for expressions of Mock T cells (mean±SEM, n=6). TCR:ICOS variant with red square was used as basis for further experimentation. **(c)** Identification of single amino acids within mCD3ε that are required for surface expression of hTCR:ICOS. Left plot: amino acid

1041 (aa) alignment between human and mouse CD3ε and overview of all single substituent
1042 mutants made. Right plot: surface expression of hTCR:ICOS with human to mouse CD3ε aa
1043 substitutes according to % TCR-Vß14, after correction for Mock (mean±SEM, n=2-10).
1044 Statistical significance between modified TCR:ICOS variants and hTCR:ICOS was assessed
1045 using a Student's t-test. Again, the TCR:ICOS variant with red square was used as basis for
1046 further experimentation. **(d)** Demonstration of antigen reactivity, sensitivity and resistance
1047 against exhaustion upon repeated stimulation of hTCR:ICOS-RA. 1st plot from the left: bar
1048 graph displaying surface expression of gp100 wt hTCR, hTCR:ICOS, and hTCR:ICOS-RA
1049 according to % TCR-Vß14 after correction for expression on mock T cells (mean±SEM, n=10).
1050 Statistical significance was calculated using a Sidak-Holm's test. 2nd plot: IFN-γ production
1051 following stimulation with T2 cells that were pre-loaded with titrated amounts of human gp100
1052 peptide. TCR T cells were co-cultured with peptide-loaded T2 cells for 16h at 37°C and
1053 supernatants were assayed using an IFN-γ ELISA (mean±SEM, n=4). EC50 values,
1054 mentioned in the plot, were calculated using graphpad prism. 3rd plot: bar graph displaying
1055 IFN-γ production of TCR T cells following stimulation with BLM tumor cells. TCR T cells were
1056 co-cultured with BLM cells that either expressed the human gp100 antigen or not for 16h at
1057 37°C, after which supernatants were assayed by ELISA for IFN-γ (mean±SEM, n=4).
1058 Statistical significance between hTCR:ICOS and wt TCR was accessed by two-way ANOVA.
1059 4th plot: T cells were co-cultured with BLM tumor cells expressing the human gp100 antigen
1060 coupled to eGFP, and viable tumor cells remaining were quantified using Incucyte
1061 (mean±SEM, n=3). 5th plot: T cells were repeatedly stimulated overnight with BLM tumor cells
1062 expressing the human gp100 antigen, with the percentage of TCR+ CD8 T cells co-expressing
1063 PD1 and TIM3 after each cycle being measured by flow cytometry (mean±SEM n=3).
1064 Statistical significance between TCR:ICOS and wt TCR T cells was tested using a two-way
1065 ANOVA with Sidak's post-hoc testing. **(e,f)** The hTCR:ICOS format with R54A is extendable
1066 to other TCR specificities, as shown for TCRs specific for NY-ESO1/A2 **(e)** and ROPN1/A2
1067 **(f)**. **(e)** 1st plot from the left: bar graph displaying surface expression of wt TCR and TCR:ICOS
1068 according to % TCR-Vß13.1 after correction for Mock (mean±SEM, n=6-12). Statistical

1069 significance between hTCR:ICOS-RA and wt TCR was assessed according to Sidak-Holm's.
1070 2nd plot: IFN-γ production following stimulation with T2 cells that were pre-loaded with titrated
1071 amounts of peptide (mean±SEM, n=7). 3rd plot: bar graph displaying IFN-γ production
1072 following stimulation with human MM-231-NY-ESO1 cells (mean±SEM, n=3). 4th panel: line
1073 graph displaying killing of MM-231-NY-ESO1 cells by T cells (mean±SEM, n=3). 5th panel:
1074 change in percentage of PD1+, TIM3+ TCR+ CD8 T cells following repeated 24h stimulations
1075 with MM-231-NY-ESO1 cells (mean±SEM, n=5). **(f)** 1st plot: bar graph displaying surface
1076 expression of wt TCR and TCR:ICOS according to % TCR-Vß13.1 after correction for Mock
1077 (mean±SEM, n=4-8). Statistical significance between hTCR:ICOS-RA and wt TCR was
1078 assessed according to Sidak-Holm's. 2nd plot: IFN-γ production following stimulation with T2
1079 cells that were pre-loaded with titrated amounts of peptide (mean±SEM, n=4). 3rd plot: bar
1080 graph displaying IFN-γ production following stimulation with human MM-231-ROPN1 cells
1081 (mean±SEM, n=2-4). 4th panel: line graph displaying killing of MM-231-ROPN1 cells by T cells
1082 (mean±SEM, n=6). 5th panel: change in percentage of PD1+, TIM3+ TCR+ CD8 T cells
1083 following repeated 24h stimulations with MM-231-ROPN1 cells (mean±SEM, n=3). With * =
1084 $p<0.05$, ** = $p<0.01$, *** = $p<0.001$.

1085